Discovery of Compounds Inhibiting the ADP-Ribosyltransferase Activity of Pertussis Toxin

Ashok, Yashwanth; Miettinen, Moona; Kimio Hirabae de Oliveira, Danilo; Tamirat, Mahlet Z.; Näreoja, Katja; Tiwari, Avlokita; Hottiger, Michael O.; Johnson, Mark S.; Lehtiö, Lari; Pulliainen, Arto T.

Published in:
ACS Infectious Diseases

DOI:
10.1021/acsinfecdis.9b00412

Published: 01/01/2020

Document Version
Accepted author manuscript

Document License
Publisher rights policy

Discovery of compounds inhibiting the ADP-ribosyltransferase activity of pertussis toxin

Yashwanth Ashok[a,#], Moona Miettinen[b,c,#], Danilo Kimio Hirabae de Oliveira[a], Mahlet Z. Tamirat[d], Katja Näreoja[b], Avlokita Tiwari[b], Michael O. Hottiger[e], Mark S. Johnson[d], Lari Lehtiö[a,*] & Arto T. Pulliainen[b,*]

[a]Faculty of Biochemistry and Molecular Medicine, Biocenter Oulu, University of Oulu, Aapistie 7A, P.O. Box 5400, FI-90014, Oulu, Finland

[b]Institute of Biomedicine, Research Center for Cancer, Infections, and Immunity, University of Turku, Kiinamyllynkatu 10, FI-20520, Turku, Finland

[c]Turku Doctoral Programme of Molecular Medicine (TuDMM), University of Turku, Turku, Finland

[d]Structural Bioinformatics Laboratory, Biochemistry, Faculty of Science and Engineering, Åbo Akademi University, Tykistökatu 6A, FI-20520, Turku, Finland

[e]Department of Molecular Mechanisms of Disease, University of Zurich, Winterthurerstrasse 190, 8057, Zurich, Switzerland

[#] Equal contribution

[*] Corresponding authors (Lari.Lehtio@oulu.fi, arto.pulliainen@utu.fi)

ABSTRACT

Targeted pathogen-selective approach to drug development holds promise to minimize collateral damage to the beneficial microbiome. The AB_5-topology pertussis toxin (PtxS1-S5) is a major virulence factor of *Bordetella pertussis*, the causative agent of the highly contagious respiratory disease whooping cough. Once internalized into the host cell, PtxS1 ADP-ribosylates α-subunits of the heterotrimeric Gαi-superfamily, thereby disrupting G-protein-coupled receptor signaling. Here, we report the discovery of the first small molecules inhibiting the ADP-ribosyltransferase activity of pertussis toxin. We developed protocols to purify mg-levels of active recombinant *B. pertussis* PtxS1 from *Escherichia coli* and an *in vitro* high throughput-compatible assay to quantify NAD^+ consumption during PtxS1-catalyzed ADP-ribosylation of Gαi. Two inhibitory compounds (NSC228155 and NSC29193) with low micromolar IC_{50}-values (3.0 µM and 6.8 µM) were identified in the *in vitro* NAD^+ consumption assay that also were potent in an independent *in vitro* assay monitoring conjugation of ADP-ribose to Gαi. Docking and molecular dynamics simulations identified plausible binding poses of NSC228155 and in particular of NSC29193, most likely owing to the rigidity of the latter ligand, at the NAD^+-binding pocket of PtxS1. NSC228155 inhibited the pertussis AB_5 holotoxin-catalyzed ADP-ribosylation of Gαi in living human cells with a low micromolar IC_{50}-value (2.4 µM). NSC228155 and NSC29193 might prove useful hit compounds in targeted *B. pertussis*-selective drug development.

Keywords: whooping cough, pertussis toxin, ADP-ribosylation, ADP-ribosyltransferase, inhibitor, drug development

INTRODUCTION

Whooping cough, i.e. pertussis, is a globally distributed acute respiratory disease [1]. Whooping cough affects all age groups [1]. However, young children are the most affected age group where the disease may lead to death despite hospital intensive care and use of antibiotics [1]. Worldwide estimates of cases and deaths in children younger than 5 years in 2014 were 24.1 million and 160.700, respectively [2]. Despite efficient global vaccine campaign whooping cough remains endemic and recent data, e.g. from USA [3], indicate that the number of cases is increasing. Moreover, macrolide resistant *B. pertussis* strains have been reported [4, 5]. Sizeable outbreaks have also been witnessed [1], but the reasons for the resurgence are incompletely understood. On the one hand, improved diagnostics and surveillance methods as well as increased awareness of whooping cough by health care professionals might contribute [1]. On the other hand, molecular changes in the pathogenic *B. pertussis* lineages and waning immunity especially after receipt of acellular pertussis vaccines have been debated [1]. In addition, acellular pertussis vaccines do not prevent infection or transmission although they protect from severe symptoms of infection based on experimentation in a nonhuman primate model [6]. These data highlight the need to improve the vaccine formulations and vaccination campaigns, but also to develop alternative means to treat whooping cough.

Pertussis toxin is a major virulence factor of *B. pertussis* [7], and a detoxified form of the toxin is included in all acellular pertussis vaccine formulations. Clinical isolates lacking pertussis toxin have turned out to be rare [8]. When administrated systemically to experimental animals, e.g. to mice [9], pertussis toxin recapitulated the leukocytosis (increase in number of circulating white blood cells) seen in young children with whooping cough. Rats experimentally infected with *B. pertussis* developed prolonged paroxysmal coughing, but an isogenic pertussis toxin-deficient strain did not cause such pathology [10, 11]. Seven-day-old neonatal mice infected with a pertussis toxin-deficient strain of *B. pertussis* survived a challenge, which caused 100% mortality with the parental strain

[12]. Therefore, targeting of pertussis toxin might prove beneficial in the treatment of whooping cough, especially in young children who still lack the vaccine-induced protection.

Pertussis toxin is composed of five non-covalently bound subunits (PtxS1-S5), which are arranged in an AB_5-topology [13, 14]. The B_5-assembly is formed by the PtxS2-S5 subunits (PtxS2, PtxS3, 2 copies of PtxS4 and PtxS5) [13, 14]. Pertussis toxin is secreted from the bacteria via Sec-pathway and Ptl type IV secretion system [15]. The B_5-assembly mediates binding of the secreted AB_5 holotoxin on the surface of various different cell types in a carbohydrate-dependent manner [14]. Subsequent cell entry is followed by dissociation of the B_5-assembly and the PtxS1-subunit [16], which belongs to the family of ADP-ribosyltransferases (ARTs) [17]. PtxS1 ADP-ribosylates a single C-terminal cysteine residue in α-subunits of most heterotrimeric Gαi-superfamily members such as Gαi, Gαo, and Gαt [18-20]. The C-terminus of the heterotrimeric G-protein α-subunits makes functionally important contacts with the plasma membrane-localized G-protein coupled receptors (GPCRs) [21]. The bulky PtxS1-catalyzed ADP-ribose modification decouples the G-protein αi-subunit, and also the βγ-dimer, from the GPCRs and inhibits the agonist stimulation-induced signal propagation inside the cell. Depending on the target cell type, these signaling pathway disturbances result in a variety of phenotypes [7]. One phenotypic effect is reduction of chemokine-induced neutrophil migration, believed to mitigate neutrophil-mediated clearance of *B. pertussis* [22]. In addition, disruption of tight junctions between airway epithelial cells, linked to the development of pulmonary edema, and blockage of anti-inflammatory cell signaling, linked to the prolonged duration of respiratory inflammation, have been proposed [7].

In addition to *B. pertussis*, ART-toxins are key virulence factors of several pathogens such as *Corynobacterium diphthteria* (diphtheria toxin), *Vibrio cholera* (cholera toxin) and *Escherichia coli* (heat-labile enterotoxin) [17]. Selective targeting and inhibition of their ADP-ribosyltranferase

activity holds promise to interfere with disease pathology. Hit compounds inhibiting *Pseudomonas aeruginosa* ExoA-induced cytotoxicity in yeast and mammalian cell-based assays *in vitro* have been identified [23]. Virtual screening on the crystal structure of a closely related cholic toxin of *Vibrio cholera* was primarily used to design the screened compound library [24]. An *in vitro* screen utilizing recombinant *Pseudomonas aeruginosa* ExoS and its host cell target protein Ras GTPase identified inhibitors from a library of compounds either known to inhibit the ART-activity of human diphtheria toxin-like ADP-ribosyltransferases (ARTDs/PARPs) or to have similar chemical properties [25]. Hit compounds for ART-toxins of *Bacillus sphaericus*, *Clostridium difficile*, and *Clostridium botulinum* were found via *in vitro* screening of kinase inhibitors, which are typically adenosine mimics and thereby chemically related to NAD^+ [26]. Bisubstrate analogs mimicking the nicotinamide portion of NAD^+ and arginine residue of the target host cell protein have also been developed to inhibit cholera toxin [27]. In addition, structures of NAD^+- or hit compound-bound ART-toxins have allowed computational analyses to understand the binding modes and to provide rational ideas for further improvements, as in the case of cholix-toxin of *Vibrio cholera* [23, 28]. However, despite the recent advancements a rationally designed drug targeting bacterial ART-toxins has yet to reach the market.

In this study, we set out to identify small molecular weight compounds that inhibit the Gαi-specific ADP-ribosyltransferase activity of pertussis toxin, and thereby to potentially interfere with the pathological effects of pertussis toxin. We developed an *in vitro* high throughput-compatible screening assay with recombinant enzyme-substrate pair, screened a high scaffold diversity compound library in parallel to a panel of selected compounds known to inhibit the ART-activity of human ARTDs/PARPs, validated the hit compounds in independent *in vitro* assays, performed docking and molecular dynamic simulations to predict the binding modes, and evaluated the potency of the hit compounds in a living cell-based assay.

RESULTS

Purification of recombinant PtxS1 (rPtxS1) from *E. coli* – We did not succeed in purifying the full length N- or C-terminally HIS-tagged recombinant *B. pertussis* PtxS1 from *E. coli* due to weak solubility and proteolytic instability (data not shown). Therefore, we engineered a double deletion to *ptxA* resulting into expression of an N-terminally HIS-tagged version of *B. pertussis* Tohama I strain PtxS1 (Asp1-Ile187, UniProt_P04977), referred hereafter to as rPtxS1, which lacks the N-terminal secretion signal sequence as well as part of the C-terminus (Fig. 1, Fig. 2A). Structural data of the pertussis AB_5 holotoxin demonstrate that the C-terminus of PtxS1 masks the active site, and indicate that di-sulfide bond reduction (Cys41-Cys201) and significant movement of the C-terminus would be required for catalysis [13, 14]. Our C-terminal truncation exposes the ADP-ribosyltransferase catalytic site of PtxS1 including the NAD^+-binding pocket (Fig. 1) [13, 14]. Based on the previous biochemical work [29, 30], our C-terminal truncation should not affect the NAD^+ glycohydrolase activity, i.e. PtxS1-catalyzed reaction between NAD^+ and water to yield ADP-ribose and nicotinamide, but it might negatively affect the ADP-ribosylation of Gαi.

rPtxS1, as purified with metal affinity and size exclusion chromatography (SEC), is proteolytically stable and migrates between the 25 and 20 kDa protein markers in SDS-PAGE (Fig. 2B), in accordance with a theoretical size of 23.4 kDa. In order to study the oligomerization state of rPtxS1 in solution, size exclusion chromatography coupled to multi-angle light scattering (SEC-MALS) was used. Purified rPtxS1 appeared as a single peak (Fig. 2C), with an estimate of 23.0 ± 0.2 kDa in a triplicate run indicating that rPtxS1 is monomeric in solution. rPtxS1 is well folded as evidenced by a sigmoidal curve with a melting temperature (Tm) of 54.7 ± 0.2 °C in a differential scanning fluorimetry (DSF)-assay (Fig. 2D).

Analysis of the ART activity of rPtxS1 – ART activity of rPtxS1 towards Gαi was first studied with a HEK293T cell membrane preparation having an endogenous level of Gαi in an NAD^+-biotin Western blot-assay. rPtxS1 ADP-ribosylated one major protein from the complex membrane proteome (Fig. 2E). This protein migrated between the 55 and 35 kDa protein markers in SDS-PAGE (Fig. 2E), in accordance with a theoretical size of endogenous Gαi, e.g. 40.4 kDa for isoform 1 (UniProt_P63096). Next, ART activity of rPtxS1 towards Gαi was studied with recombinant N-terminally HIS-tagged Gαi (isoform 1, UniProt_P63096) purified from *E. coli*, hereafter referred to as rGαi, in an NAD^+ Western blot-assay. rPtxS1 ADP-ribosylated rGαi (Fig. 2F), indicating that Gαi may serve as a substrate without the G-protein βγ-complex or other cellular constituents. SEC-analysis of rPtxS1-rGαi complex solution topology showed the presence of only single monomeric rPtxS1 and rGαi proteins (Fig. S1). rPtxS1-rGαi complex formation during catalysis therefore appears to be weak, i.e. the rGαi modification is based on a transient kiss-and-run interaction. Interestingly, rPtxS1 modified itself (Fig. 2E), and it already had become auto-ADP-ribosylated in the *E. coli* expression host (Fig. 2F). This activity was drastically diminished in a Q127D/E129D double mutant of rPtxS1(Fig. S2A), hereafter referred to as rPtxS1-mutant. Based on a DSF-assay, the Tm of the rPtxS1-mutant was 52.0 ± 0 °C as compared to Tm of the rPtxS1-wt (Tm of 54.7 ± 0.2 °C), indicating that the Q127D/E129D double mutation does not affect the folding of rPtxS1. The rPtxS1-mutant was also incapable of ADP-ribosylating rGαi (Fig. S2B). This double mutant of rPtxS1 was analyzed, because structurally identical mutations in a recently discovered pertussis-like toxin from *E. coli* caused catalytic inactivation, although NAD^+ was still capable of binding to the protein (Fig. S2C) [31]. Q127 and E129 of rPtxS1 are also conserved with several other bacterial ART-toxins where these residues position NAD^+, in particular the nicotinamide end (Fig. S2C), and promote the transfer of ADP-ribose to a substrate amino acid residue [17]. To assess the substrate

amino acid specificity of the extensively truncated rPtxS1 (see Fig. 1 and Fig. 2A), we analyzed the C351A mutant of rGαi (UniProt_P63096), hereafter referred to as rGαi-mutant, in an NAD^+-biotin Western blot-assay. rPtxS1 ADP-ribosylated rGαi, but it was incapable of ADP-ribosylating the rGαi-mutant (Fig. S3). Based on a DSF-assay, the Tm of the rGαi-mutant was 44.3 ± 0.2 °C as compared to Tm of the rGαi-wt (Tm of 43.8 ± 0.2 °C), indicating that the C351A mutation does not affect the folding of rGαi. Therefore, rPtxS1 is not only catalytically active towards rGαi, but it retains the Gαi substrate amino acid specificity evidenced with the pertussis AB_5 holotoxin [18-20].

Multiwell-based assay set-up for screening of rPtxS1 inhibitors – We analyzed the suitability of a fluorometric method to screen for rPtxS1 inhibitors previously developed for poly-ADP-ribose (PAR) synthesizing enzymes [32] and later extended to mono-ADP-ribose (MAR) synthesizing enzymes [33, 34]. The end point assay is based on conversion of NAD^+ to a stable fluorophore with emission maximum at 444 nm [32]. The decrease in fluorescence in comparison to the non-enzyme control is a measure of NAD^+-consuming enzymatic activity [32]. Incubation of rPtxS1 with rGαi for 40 min resulted in a strong decrease of fluorescence (Fig. 3A). No fluorescence decrease was detected with the rPtxS1-mutant under identical conditions (Fig. 3A). Reactions with different concentrations of rPtxS1 were stopped at various time points to measure NAD^+ consumption in the presence of a constant amount of rGαi substrate. These data demonstrated that an increase in the rPtxS1 concentration increases NAD^+ consumption that also progresses over time (Fig. 3B). rPtxS1 could also consume NAD^+ in the absence of rGαi, although much slower than with the rGαi substrate (Fig. 3A). This NAD^+ glycohydrolase activity was not detected with the rPtxS1-mutant (Fig. 3A). The effect of dimethyl sulfoxide (DMSO) on the NAD^+-consuming activity of rPtxS1 was also studied because small molecules in chemical libraries are usually dissolved in DMSO

typically resulting in assay concentrations of 0.1% – 1% DMSO. DMSO did not have a significant effect on the NAD^+-consuming activity of rPtxS1 in the presence of rGαi substrate up to 0.2% DMSO, while 1% DMSO already significantly ($p = 10^{-4}$) reduced activity (Fig. 3C). We chose to perform compound screening for rPtxS1 inhibitors in the presence of 0.1% DMSO. To test reproducibility of the fluorometric assay, maximum (NAD^+ as incubated in plain buffer) and minimum (NAD^+ as incubated in rPtxS1- and rGαi-containing buffer) signals were measured from five independent runs to test plate-to-plate and day-to-day variability. The average Z' value for the assay was 0.68, indicating that the fluorometric assay is suitable for high throughput screening. The statistical parameters of the NAD^+ quantitation assay are summarized in Table S1.

Screening for rPtxS1 inhibitors – We first analyzed a panel of selected compounds (n = 32) known to inhibit the ART-activity of human diphtheria toxin-like ADP-ribosyltransferases (ARTDs/PARPs). These compounds (Table S2), which also included several FDA-approved anti-cancer drugs such as Rucaparib, did not inhibit the NAD^+-consumption activity of rPtxS1 in the presence of rGαi (arbitrary inhibitory threshold = 50%). Next, we screened a diversity set compound library obtained from the National Cancer Institute (NCI) Developmental Therapeutics program repository (https://dtp.cancer.gov), which at the time of acquiring contained 1,695 compounds (diversity set III). The so-called diversity set contains selected compounds, e.g. to represent high scaffold diversity, from the over 100,000 NCI-repository compounds. A total of nine compound hits were identified, which inhibited the NAD^+-consumption activity of rPtxS1 in the presence of rGαi more than 50%. These nine compounds were analyzed in an independent NAD^+-biotin Western blot-assay, which measures the rPtxS1-catalyzed conjugation of ADP-ribose-biotin onto rGαi. Five out of the nine primary compound hits showed strong inhibition of rPtxS1-catalyzed rGαi ADP-ribosylation (Fig. 4A, titration effect shown for NSC228155 and NSC29193

in Fig. 4B). NSC119875 (Cisplatin, DNA alkylating agent used in cancer treatments) and NSC44750 affected rGαi and/or rPtxS1 protein integrity in the NAD^+-biotin Western-blot based assay (Fig. 4A), even if the assay was performed with a 10-fold lower compound concentration (data not shown). NSC119875 and NSC44750 were therefore excluded from further studies. To evaluate the potency of the remaining three compounds to inhibit rPtxS1, dose response studies were performed using the fluorometric NAD^+-consumption assay in the presence of rGαi. NSC228155 and NSC29193 had IC_{50}-values of 3.0 and 6.8 μM, respectively (Fig. 4C). NSC149286 was less potent than the other two compounds with an IC_{50}-value of 20 μM (Fig. 4C), and was excluded from further analyses. Chemical structures of the hit compounds are shown in Figure 4C. NSC228155 and NSC29193 appeared to have mimicry to the adenine base or the nicotinamide end of NAD^+ (Fig. 4D). We also utilized an alternative readout of the NAD^+-biotin assay, i.e. capture of HIS-tagged proteins on 96-well nickel-coated plates followed by the detection of protein-conjugated ADP-ribose-biotin. NSC228155 and NSC29193 showed strong inhibition of the rPtxS1-catalyzed conjugation of ADP-ribose-biotin onto rGαi (Fig. 4E). NSC228155 and NSC29193 also inhibited the auto-ADP-ribosylation activity of rPtxS1 (Fig. 4F), indicating that these two compounds interact directly with rPtxS1. The two hit compounds were not identified as pan-assay interference compounds or aggregators (zinc15.docking.org). In summary, compound screening resulted into identification of NSC228155 and NSC29193, which inhibited the ART activity of rPtxS1 in low micromolar concentrations.

Putative binding poses of NSC29193 and NSC228155 to PtxS1 – In order to evaluate possible binding modes of the compounds to PtxS1, we performed docking and molecular dynamic simulation (MDS) (Fig. 5, Fig. S4, Fig. S5). The top ranked poses of NSC228155 shared features, including the placement of the aromatic pyridine ring of NSC228155 in an enclosed region where

the nicotinamide ring of NAD^+ would bind to PtxS1, with the double benzoxadiazole ring positioned near the center of the NAD^+-binding pocket. The benzoxadiazole ring is joined to the pyridine ring via a central sulfur atom, and the rotatable bonds permit the adoption of varying conformations. In pose 1 (Fig. 5A), with the lowest free energy of binding (ΔG_{bind} of -51.2 kcal/mol; docking score of -4.08 kcal/mol), the pyridine ring oxygen of the ligand forms a hydrogen bond with the main-chain nitrogen atom of Tyr10, anchoring the ligand to an aromatic area of the binding pocket, and with π-π stacking interactions observed for the pyridine ring with nearby Tyr59 and for the benzoxadiazole ring with Tyr63. In pose 2 (Fig. S5A), having the best docking score (-4.20 kcal/mol; ΔG_{bind} of -43.3 kcal/mol), the pyridine ring is rotated 90° relative to pose 1, losing the backbone hydrogen bond with Tyr10, but making π-π interactions with both Tyr63 and Tyr10, and ionic interactions with Arg9 and Arg67. In MDS, pose 1 showed stability and retained its position with respect to the original docked position, only differing on average by an root-mean-square deviation (RMSD) of 0.9 Å (Fig. S4A), and the RMSD for the ligand orientations differ on average by 2.3 Å when the coordinates of PtxS1 are superposed over the backbone atoms. In contrast, pose 2 was unstable at the initial binding position and occupied different locations of the binding pocket with an average 22 Å RMSD for the ligand based on superposing the PtxS1 coordinates from the simulation (Fig. S4B).

In contrast to NSC228155, NSC29193 is rigid and almost exclusively resulted in two docked poses. Pose 1 of NSC29193 (Fig. 5B) is positioned near the binding site for the nicotinamide ring of NAD^+ in the PtxS1, hydrogen bonding with main-chain nitrogen and oxygen atoms of Tyr10. Additionally, NSC29193 forms π-cation interactions with Arg9, π-π stacking with Tyr63 and hydrogen bonding with the side-chain hydroxyl group of Ser52. NSC29193, pose 2, is bound near the location where the adenine ring of NAD^+ would be bound in the pertussis toxin, stacking against the aromatic ring of Trp26 and hydrogen bonding with the main-chain oxygen atom of Thr24 (Fig.

S5B) as well as forming ionic interactions with Arg9 and Arg13 via the lone pair electrons of the nitrogen atom on the five-member ring. During MDS, NSC29193 pose 1 was quite stable, with an average RMSD of 0.1 and 1.0 Å with respect to the ligand and receptor backbone atoms (Fig. S4C), and interactions between the ligand and main-chain atoms of Tyr10 were conserved for over 90% of the simulation time. The π-π interactions with Tyr63 and π-cation interactions with Arg9 were also retained for the majority of the simulation time. In contrast, the binding mode of pose 2 was disrupted at around 20 ns of the simulation (Fig. S4D), mainly due to the reorientation of the indole ring of Trp26, which appears to be one of the key interaction partners of NSC29193. Consequently, in pose 2 the ligand moves from the initial binding position and binds to several areas of the binding pocket. This is reflected by the average 12 Å RMSD of the ligand with respect to the superposed coordinates of the toxin from the simulation (Fig. S4D). Taken together, docking and MDS resulted in identification of plausible binding poses of NSC228155 and in particular for NSC29193, most likely owing to the rigidity of the latter ligand, at the NAD^+-binding pocket of PtxS1.

NSC228155 and NSC29193 as inhibitors of pertussis toxin in living human cells – First, to find the optimal toxin dosage, we titrated the pertussis AB_5 holotoxin and detected the ADP-ribosylation of endogenous Gαi by Western blot-assay using a polyclonal MAR-recognizing antibody. Incubation of HEK293T cells for 2 h with the holotoxin resulted, in a concentration dependent-manner, in mono-ADP-ribosylation of a single protein migrating between the 35 and 55 kDa protein markers in SDS-PAGE (Fig. 6A), in accordance with a theoretical size of endogenous Gαi, e.g. 40.4 kDa for isoform 1 (UniProt_P63096). Next, we pre-incubated the HEK293T cells for 30 min with the compounds NSC228155 or NSC29193 prior to addition of the holotoxin and subsequent co-incubation. We did not detect inhibitory action for the compound NSC29193 despite multiple analyzed conditions (data not shown), e.g. i) 30 min pre-incubation with inhibitor (0.1, 1,

10 and 50 µM) + 2 h with holotoxin (10 ng/mL) or ii) 1, 2, 3, 4 and 5 h pre-incubation with 50 µM inhibitor + 2 h with holotoxin (10 ng/mL). However, compound NSC228155 inhibited the Gαi-specific ADP-ribosylation activity of holotoxin in a concentration-dependent manner (Fig. 6B). Some inhibitory action was evidenced with 0.1 and 1 µM of NSC228155, but 5 µM of NSC228155 resulted approximately in 80% inhibition of mono-ADP-ribosylation of Gαi. Based on pixel intensity analysis of the anti-MAR signal, the IC_{50} of NSC228155 inhibitory effect was 2.35 µM (Fig. 6C). NSC228155 did not lower the amount of cell-associated PtxS1 or the proteolytic processing of PtxS1 (Fig. S6), which has been proposed to happen at an early endocytic step of the pertussis toxin internalization [35]. Furthermore, NSC228155 did not affect cellular localization, including accumulation close to the nuclei where endoplasmic reticulum resides, of the widely used retrograde trafficking marker Alexa594-conjugated cholera toxin B5-oligomer (Fig. S7). Therefore, it appears that NSC228155 inhibits the pertussis toxin-mediated ADP-ribosylation of Gαi with a neglectable effect on the retrograde endosomal trafficking process of pertussis toxin.

Having established NSC228155 as a potent inhibitor of pertussis toxin in living HEK293T cells, we turned our attention to the maximum tolerated dose. NSC228155, at the effective 5 µM inhibitory concentration, did not significantly induce the DNA-damage induced PARP1 (also called ARTD1) poly-ADP-ribosylation (Fig. 6D), cell death-associated PARP1/ARTD1 proteolytic processing from the approximately 120 kDa full length form into the approximately 90 kDa form (Fig. 6D), or the cell death-associated nuclear fragmentation (Fig. S7). However, visual alterations, including partial cell detachment, was detected in HEK293T cell monolayers upon titration of NSC228155 up to 50 µM in the 2.5 h Gαi ADP-ribosylation assay (data not shown). Therefore, we utilized the MTT-assay, i.e. reduction of tetrazolium salt into formazan by metabolically active cells, to study the potential cytotoxicity of NSC228155. The metabolic activity of HEK293T cells, as analyzed by the MTT-assay 3.5 h after addition of NSC228155, was

significantly affected with 20 μM or higher concentrations (Fig. 6E). IC_{50} of NSC228155 cytotoxicity was 15.33 μM (Fig. 6E). In conclusion, NSC228155 is a potent inhibitor of pertussis toxin in living HEK293T cells, but at high concentrations it induces cytotoxicity. The mechanism(s) of NSC228155 cytotoxicity needs to be addressed in the future hit development of NCS228155.

DISCUSSION

We report the identification of the first small molecular weight compounds inhibiting the ADP-ribosyltransferase activity of pertussis toxin *in vitro* and in living cells. ADP-ribosyltransferase activity of pertussis toxin is important for the pathological effects of pertussis toxin. Seven-day-old neonatal mice infected with a *B. pertussis* strain expressing a mutant of PtxS1 lacking the ART-activity fully survived a challenge, which caused 100% mortality with the parental strain of *B. pertussis* [12]. Purified AB_5 holotoxin containing the same PtxS1 mutant was incapable of inducing leukocytosis in mice in doses that were 100-fold more than the median lethal dose of wild-type AB_5 holotoxin [36]. Therefore, targeting of the ADP-ribosyltransferase activity of pertussis toxin might prove beneficial in the treatment of whooping cough.

Compound library screening was made possible due to our ability to purify mg-levels of active recombinant *B. pertussis* PtxS1 (rPtxS1) from *E. coli*. rPtxS1 retained the high amino acid specificity of pertussis AB_5 holotoxin toward the single C-terminal cysteine in Gαi [18-20]. Used truncation positions in rPtxS1 are functionally justified. PtxS1 contains an N-terminal signal sequence ending at Ala34 [37, 38] that gets cleaved upon the Sec-mediated secretion of PtxS1 from the cytoplasm into the periplasm where the AB_5 holotoxin is assembled prior to Ptl type IV secretion system-mediated export. The truncated part of the PtxS1 C-terminus masks the NAD^+-binding pocket in the AB_5 holotoxin involving a stabilizing intramolecular di-sulfide bond between Cys41 and Cys201 [13, 14]. Our truncation approach bypasses the need for disulfide bond reduction [39] and extensive conformational movement of the C-terminus [13, 14] to activate PtxS1, which inside the host cell has also been proposed to involve proteolysis [35].

We made an initial attempt to identify PtxS1 inhibitory compounds from molecules (n = 32, see Table S2) known to inhibit the ART-activity of human diphtheria toxin-like ADP-ribosyltransferases (ARTDs/PARPs). We envisioned that some of these compounds, which target

356 the ARTD/PARP NAD^+-binding pockets, could provide a fast track to drug development via
357 repurposing drug strategy, due to the current FDA-approvals in cancer therapy. However, none of
358 these compounds significantly inhibited the NAD^+-consumption activity of rPtxS1 in the presence
359 of rGαi. Therefore, we decided to screen a diversity set compound library (n = 1,695) obtained
360 from the National Cancer Institute (NCI) Developmental Therapeutics program repository
361 (https://dtp.cancer.gov). Two potent inhibitory compounds NSC29193 and NSC228155 with low
362 micromolar IC_{50}-values were identified in the *in vitro* NAD^+ consumption assay. These
363 compounds were also potent in an independent *in vitro* assay where we monitored the amount of
364 rGαi-conjugated ADP-ribose-biotin upon rPtxS1 catalysis by streptavidin-HRP Western blotting
365 (see Fig. 4B). NSC228155 and NSC29193 also inhibited the auto-ADP-ribosylation activity of
366 rPtxS1 (see Fig. 4F), indicating that these two compounds interact directly with rPtxS1. Our
367 docking and molecular dynamic simulations resulted in plausible binding poses for both ligands
368 NSC228155 and NSC29193 (see Fig. 5 and S4). More consistent, energetically favorable binding
369 poses were observed for NSC29193. This appears to be in accordance with the compound
370 structures (see Fig. 4C). NSC29193 (purine-2,8-dithiol) is a rather rigid purine analogue that
371 mimics the structure of the adenine base of NAD^+ (see Fig. 4D). NSC228155, on the other hand,
372 contains two major molecular structures, connected by a rotatable linker, one ring compound
373 mimicking the adenine base of NAD^+ and the other ring compound mimicking the nicotinamide of
374 NAD^+. It is noteworthy that 7 other compounds were also positive in the *in vitro* NAD^+
375 consumption assay, some apparently via deleterious effects for protein stability as evidenced by
376 the independent *in vitro* ADP-ribose conjugation assay (see Fig. 4A), i.e. compounds NSC44750
377 and NSC119875 (cisplatin). The data highlights the importance of validating the primary screening
378 hits in alternative and independent *in vitro* assays. In summary, compound screening resulted into

379 the identification of two compounds, NSC29193 and NSC228155, which inhibited the rPtxS1-
380 catalyzed ADP-ribosylation of rGαi *in vitro* with low micromolar IC_{50}-values.

381 NSC228155, but not NSC29193, was a potent inhibitor of pertussis holotoxin-mediated ADP-
382 ribosylation of Gαi in living HEK293T cells. We analyzed multiple different experimental set-ups
383 with NSC29193, including concentrations up to 50 µM that did not cause visible alterations or cell
384 detachment of HEK293T cell monolayers. In respect of previous drug screening approaches there
385 appears to be no published information on NSC29193. Accordingly, the cell permeability of
386 NSC29193 is not known, but might be weak and thus explain our negative inhibitory data. In sharp
387 contrast, we detected approximately 80% inhibition of the Gαi ADP-ribosylation with 5 µM
388 NSC228155 (see Fig. 6C). In part, this could relate to the fact that NSC228155 easily permeates
389 cells. It has been shown in MDA-MB-468 breast cancer cells that 5 min incubation with 100 µM
390 NSC228155 caused rapid movement of this inherently fluorescent molecule across cell membranes
391 and dispersal to both the cytoplasm and nucleus [40]. However, we witnessed significant toxicity of
392 NSC228155 for HEK293T cells with 20 µM or higher concentrations after a 3.5-h incubation
393 (cytotoxicity IC_{50} – 15.33 µM see Fig. 6E). This cytotoxicity might be caused by the proposed
394 NSC228155-mediated production of reactive oxygen species (ROS) inside the cell [40]. In this
395 respect, it is noteworthy that, upon incubation of cells with 5 µM of NSC228155 for 2.5 h, we did
396 not detect auto-ADP-ribosylation of PARP1/ARTD1 (see Fig. 6D), which is induced in cells upon
397 ROS-induced DNA damage [41]. Moreover, we did not detect caspase-mediated proteolytic
398 PARP1/ARTD1 cleavage (see Fig. 6D), which is a robust readout for the onset of programmed cell
399 death. However, future hit development needs to address the apparent cell toxicity effects of
400 NCS228155 at high concentrations. Medicinal chemistry efforts including molecular modeling and
401 crystallography could be employed to help to design less toxic NCS228155 analogs, and with
402 additionally increased potency and specificity to inhibit PtxS1. Taken together, NSC228155 is a

potent cell permeable hit compound to inhibit pertussis holotoxin-mediated ADP-ribosylation of Gαi in living cells in low micromolar concentrations.

Resurgence of whooping cough has been witnessed even in highly vaccinated populations [1-3], and currently there are no specific drugs to treat whooping cough. Macrolide antibiotics, when administrated at a very early stage, show therapeutic effects in certain patient subgroups such as in infants <3 months of age [42]. However, macrolide resistant *B. pertussis* strains have been reported [4, 5]. Targeting of pertussis toxin, the major virulence factor of *B. pertussis* [7], might prove beneficial in the treatment of whooping cough. Humanized monoclonal antibodies have been developed that block pertussis toxin cell surface receptor interaction or the subsequent internalization and retrograde trafficking [43]. These humanized antibodies prevented the characteristic signs of whooping cough in mouse and baboon models [44]. Our current study shows that small molecular weight compounds inhibiting the ADP-ribosyltransferase activity of pertussis toxin might also have therapeutic potential.

CONCLUSION

We conclude that NSC228155 and NSC29193 are useful templates for hit development to specifically inhibit pertussis toxin ADP-ribosyltransferase activity in whooping cough. We envision that especially young children who still lack the vaccine-induced protection against whooping cough could benefit from pertussis toxin inhibitors, administered either systemically or via inhalation. The young whooping cough patients, in contrast to adults, are typically diagnosed very early and thereby could possess a therapeutic window to interfere with the pertussis toxin-induced pathology. Exposed family members of the whooping cough patients could be an additional patient group subjected to a prophylactic administration of pertussis toxin inhibitors, possibly in combination with macrolide antibiotics.

EXPERIMENTAL SECTION

Expression plasmids – ***i) rPtxS1-wt*** Synthetic DNA fragment (Eurofins Genomics) encoding for amino acids D35-I221 of *Bordetella pertussis* strain Tohama I (UniProt_P04977) was cloned with NdeI and BamHI into pET15b (Novagen) allowing expression of an N-terminally HIS-tagged rPtxS1 (MGSSHHHHHHSSGLVPRGSHM-D35-PtxS1-I221). The D35-I221 truncation positions of PtxS1 are based on [30]. Of note, Asp35 is classically numbered as the first amino acid of PtxS1. ***ii) rPtxS1-Q127D/E129D*** pET15b-rPtxS1 plasmid was linearized with PCR using 5'-phosphorylated oligonucleotide primers (Eurofins Genomics) prAPV-351 (GATAGCGATTATCTGGCACACCGGCGCATTCCG, mutagenic nucleotides underlined) and prAPV-352 (GTAGGTGGCCAGCGCGCCGGCGAGGATACG). The PCR product was gel-isolated, re-ligated and transformed to acquire the mutant plasmid. ***iii) rGαi-wt*** Synthetic DNA fragment (GenScript) encoding for *E. coli* codon-optimized full-length human Gαi (isoform 1, UniProt_P63096-1) was cloned into pNIC-Bsa4 (Structural Genomics Consortium) using the ligation independent cloning method allowing expression of an N-terminally HIS-tagged rGαi (MHHHHHHSSGVDLGTENLYFQS-Gαi). ***iii) rGαi-Cys351Ala*** rGαi-encoding plasmid was used as a template in PCR to amplify Cys351Ala-mutant-encoding mutant allele using oligonucleotide primers (Eurofins Genomics) prAPV-418 (tacttccaatccATGGGTTGCACCCTGAGCGCGGAA, LIC-cloning overhangs in lowercase) and prAPV-419 (tatccacctttactgTCAGAACAGGCCCGCATCCTTCAGGTTGTTCTTG, mutagenic nucleotides underlined, LIC-cloning overhangs in lowercase). The PCR product was cloned into pNIC-Bsa4 (Structural Genomics Consortium) using the ligation independent cloning method allowing expression of an N-terminally HIS-tagged rGαi-Cys351Ala mutant similar to rGαi-wt. All expression plasmids were verified by sequencing.

Protein expression and purification – Expression plasmids were transformed into BL21(DE3) (Novagen) and selected overnight at 37°C on Luria-Bertani (LB) agar with appropriate antibiotics. Next morning, the bacterial lawn from the LB-plates was transferred into Terrific broth autoinduction medium (Formedium, AIMTB0205) supplemented with 0.8% (w/v) of glycerol with appropriate antibiotics. Cultures were grown at 37°C with 250 rpm until optical density at 600 nm reached 1 (typically 3-5 h), and temperature was reduced to 18°C. Bacteria were collected after 24 h by centrifugation and were either frozen to -80°C as pellets, in lysis buffer or directly used for purification. Pefabloc protease inhibitor (Roche, 11585916001) was added to 0.1 mM in the thawed biomass in lysis buffer [100 mM Hepes (pH 7.5), 500 mM NaCl, 10% (w/v) glycerol, 0.5 mM Tris(2-carboxyethyl)phosphine hydrochloride (TCEP), 10 mM imidazole]. Samples were sonicated and clarified by centrifugation. Supernatant was loaded to 5 mL HisTrap HP column (GE Healthcare). With rPtxS1 proteins, column was washed with 10 column volumes of wash buffer I and II. Wash buffer I and II have identical compositions to lysis buffer with the exception of imidazole concentration of 25 and 50 mM, respectively. rPtxS1 proteins were eluted with elution buffer [100mM Hepes (pH 7.5), 500 mM NaCl, 10% (w/v) glycerol, 0.5 mM TCEP, 500 mM imidazole], concentrated using a 10 kDa cut-off concentrator (Thermo Scientific) and subjected to size exclusion chromatography on Superdex75 16/600 Hiload Superdex column (GE Healthcare) using SEC buffer [100 mM Hepes (pH 7.5), 500 mM NaCl, 10% (w/v) glycerol, 0.5 mM TCEP]. With Gαi proteins, HisTrap HP column was washed with 15 column volumes of wash buffer [20mM Hepes (pH 7.5), 500 mM NaCl, 10% (w/v) glycerol, 0.5 mM TCEP, 25 mM imidazole] and eluted with elution buffer [20 mM Hepes (pH 7.5), 500 mM NaCl, 10% (w/v) glycerol, 0.5 mM TCEP, 500 mM imidazole]. Fractions were concentrated using a 10 kDa cut-off concentrator (Thermo Scientific) and further purified by size exclusion chromatography on Superdex75 16/600

Hiload Superdex column (GE Healthcare) with SEC buffer [30 mM Hepes (pH 7.5), 350 mM NaCl, 1 mM $MgCl_2$, 0.5 mM TCEP]. Protein fractions were pooled, concentrated using a 10 kDa cut-off concentrator (Thermo Scientific), flash frozen and stored in -80°C.

Multi-angle light scattering – All experiments were conducted with SEC-MALS buffer [100 mM Hepes (pH 7.5), 500 mM NaCl, 10% (w/v) glycerol, 0.5 mM TCEP] with a flow rate of 0.150 mL per minute. Buffer was filtered with 0.1 µm filter to remove small particles. Typically 100 µg of protein samples were injected into Superdex 200 10/300 increase column (GE Healthcare) by a Shimadzu autosampler coupled HPLC machine. Light scattering data were recorded using a multiangle light scattering detector (miniDAWN TREOS, Wyatt technology). Data were analyzed using Astra software (Wyatt technology). For complex formation studies, 100 µg of rPtxS1 and 100 µg of rGαi was incubated on ice for 2 h and then injected into the column.

Differential scanning fluorimetry (DSF) – rPtxS1 at a concentration of 0.25 mg/mL was used in PBS [phosphate buffered saline; 2 mM NaH_2PO_4, 8 mM Na_2HPO_4, 137 mM NaCl, pH 7.2]. Protein was incubated with 5 × SYPRO orange (Thermo Scientific) for 10 minutes. The samples were heated from 20-90°C with 1°C increments (1 min/1°C). The experiment was run on 2500 Real-Time PCR systems (Applied Biosystems). The resulting data was analyzed with Boltzmann sigmoidal equation using GraphPad (GraphPad software, Inc.). Thermal stability of rGαi, rGαi-mutant and rPtxS1 alone as well as in the presence of NSC228155 or NSC29193, was analyzed by DSF using a CFX96 Real-Time PCR detection system (Bio-Rad). rGαi, rGαi-mutant and rPtxS1 at a concentration of 0.2 mg/mL was used in 20 mM Hepes (pH 7.5), 500 mM NaCl, 10% (w/v) glycerol, 0.5 mM TCEP. The inhibitor concentrations used in the assay ranged from 50 µM to 1

497 mM. Samples were incubated with 5 × SYPRO Orange (Thermo Scientific) for 5 min. The samples
498 were heated from 20-90°C with 0.5°C increments (1 min/1°C). Tm-values were determined by
499 using the CFX96 Real-Time PCR detection system (Bio-Rad) software.
500
501 ***In vitro* ADP-ribosylation assays** – ***i) enzyme-excess condition with Western blot read-out***
502 Reactions (typically in 120 µL) contained 10 µM rPtxS1 proteins, 10 µM biotinylated NAD^+
503 (Trevigen, 4670-500-01) or 10 µM NAD^+ (Sigma, N3014) and either 4 µM rGαi proteins or
504 membrane fraction of HEK293T cells (30 µg of total protein) as the substrate in 100 mM Hepes
505 (pH 7.5), 500 mM NaCl and 10% (w/v) glycerol. The membrane fraction was prepared essentially
506 as described in [45]. 80% confluent 10 cm cell culture plate of HEK293T cells was placed on ice and
507 washed twice with PBS. Cells were collected by scraping into 1 mL of hypotonic lysis buffer [20
508 mM Hepes (pH 7.5), 2.5 mM $MgCl_2$, 1 mM DTT supplemented with Pierce Protease and
509 Phosphatase Inhibitor Mini Tablets (40 µL/mL of stock solution – one tablet / 2 mL H_2O, Thermo
510 Scientific, 88668) and 25 U/mL of benzonase (Merck-Millipore, 70664-3). The cells were
511 incubated at 4°C for 1 h in rotation to allow them to swell and partially lyse. The partial lysates
512 were drawn 20 times through 27-gauge needles and centrifuged with low speed (600 × g, 4°C, 10
513 min) to pellet the nuclei and insoluble cell debris. The low-speed supernatant was subjected to
514 high-speed centrifugation (16100 × g, 4°C, 30 min) to pellet the membranes. The membranes were
515 resolubilized into 50 µL of 50 mM Hepes (pH 7.5), 200 mM NaCl, 1 mM EDTA and 10 mM DTT,
516 0.3% (w/v) SDS and 2% Triton X-100 supplemented with protease and phosphatase inhibitors, in
517 concentration as described above. Protein concentration was measured with Bradford assay. The
518 ADP-ribosylation reactions were carried out at room temperature for 3 h with shaking at 300 rpm.
519 Reactions were stopped by addition of Laemmli loading dye to 1 × and heating for 10 minutes at

95°C. The samples were run on SDS-PAGE and transferred to nitrocellulose membranes, followed by blocking with 1% (w/v) casein blocking buffer (Bio-Rad, 161-0782). Membranes were incubated with streptavidin conjugated to horse radish peroxidase (1:5000) (GE Healthcare, RPN1231VS) in 1% (w/v) casein blocking buffer (Bio-Rad, 161-0782) for 3 h at 4°C in rotation and washed thrice with Tris-buffered saline [10 mM Tris-HCl (pH 7.5), 150 mM NaCl] containing 0.05% Tween 20 (TBST) for ten minutes each time. Alternatively, after blocking with 4% (w/v) bovine serum albumin (BSA) in TBST, membranes were probed in TBST containing 2% (w/v) BSA (24 - 48 h at 4°C in rotation) for HIS-tagged rPtxS1 and rGαi proteins with mouse monoclonal anti-HIS (1:1000) (R&D Systems, MAB050), for Gαi with mouse monoclonal anti-Gαi (1:500) (Santa Cruz Biotechnology, sc-136478) or mono-ADP-ribose with a rabbit polyclonal anti-mono-ADP-ribose (1:1000) antibody (Hottiger-laboratory). Primary antibody membranes were washed thrice with TBST containing 2% (w/v) BSA for ten minutes each time. Primary antibody membranes were incubated with mouse IgG kappa binding protein conjugated to horseradish peroxidase (1:2500) (sc-516102, Santa Cruz Biotechnology) or goat anti-rabbit IgG conjugated to horseradish peroxidase (1:2500) (sc-2004, Santa Cruz Biotechnology) for 3 h at 4°C in rotation and washed thrice with TBST for ten minutes each time. All membranes were subsequently developed with WesternBright ECL (Advansta) and imaged on ImageQuant LAS 4000 (GE Healthcare). ***ii) substrate-excess condition with Western blot read-out*** Reactions (typically in 50 µL) contained 50 nM rPtxS1 proteins and 500 nM rGαi in 50 mM sodium phosphate (pH 7.0) and 1 µM biotinylated NAD^+ (Trevigen, 4670-500-01). The reactions were carried at room temperature for 40 minutes. For validating hits from chemical screening, 10 µM of the indicated compound and 0.1% DMSO (control reaction) were used. Reactions were stopped by addition of Laemmli loading dye to 1 × and heating for 3 minutes at 90°C. The samples were run on SDS-PAGE and transferred

to nitrocellulose membranes, followed by blocking with 1% (w/v) casein blocking buffer (Bio-Rad, 161-0782). Membranes were incubated with streptavidin conjugated to horse radish peroxidase (1:7000) (PerkinElmer, NEL750001EA) in 1% (w/v) casein blocking buffer (Bio-Rad, 161-0782) for 3 h at 4°C in rotation and washed thrice with TBST for ten minutes each time. Alternatively, for anti-His blotting, Penta His HRP conjugate (Qiagen, 34460) was diluted 1:5000 in 1% (w/v) casein blocking buffer (Bio-Rad, 161-0782). Blots were incubated at room temperature for 2 h, followed by 3 washes with TBST each for 5 minutes. Membranes were subsequently developed with WesternBright ECL (Advansta) and imaged on ChemiDoc XRS+ (Bio-Rad). ***iii) substrate-excess condition with nickel-plate readout*** The enzymatic activity of rPtxS1 in the absence (automodification) or presence of rGαi (substrate protein modification) and inhibitors (NSC288155 and NSC29193) was analyzed using 500 nM rPtxS1, 2 µM rGαi and 200 µM of inhibitors in 50 mM HEPES pH 7.5, 100 mM NaCl, 4 mM $MgCl_2$ and 0.2 mM TCEP. Triplicate reactions were started at RT in PCR tubes by addition of an NAD^+-mixture resulting to final concentrations of 24.5 µM NAD^+ (Sigma, N3014) and 0.5 µM of biotinylated NAD^+ (Trevigen, 4670-500-01). Reactions were incubated in constant shaking for 30 min at RT prior to addition to white 96-well nickel-coated plates (Pierce, 15242). Reactions were incubated on the nickel-coated plates for 60 min at RT after which reactions were stopped by addition of 7 M guanidine hydrochloride. Plates were washed after 5 min incubation at RT three times with TBST after which blocking solution containing 1% (w/v) BSA in TBST was added for 40 min. After blocking with BSA, streptavidin-conjugated horseradish peroxidase (GE Healthcare, RPN1231VS) in TBST-BSA was added (1:5000) for 60 min. Plates were washed four times with TBST after which chemiluminescent substrate (Advansta, WesternBright Quantum) was added and subsequent chemiluminescence was detected using Hidex Sense microplate reader (Hidex).

In vitro* NAD$^+$ consumption assay** – ***i) basic reaction set-up Reactions were carried out in a U-shaped 96-well black plate (Greiner BioOne, 650209). Typically, reactions were conducted with 50 mM sodium phosphate (pH 7.0) at 25°C with shaking at 300 rpm with a reaction volume of 50 µL. The reactions were stopped by adding 20 µL of 20% acetophenone (diluted with ethanol) and 20 µL of 2M KOH and incubated at room temperature for 10 minutes. 90 µL of formic acid was added and further incubated for 20 minutes. The plates were read using Tecan infinity M1000 pro with excitation and emission wavelengths set at 372 and 444 nm, respectively. Maximum signal was defined as the NAD$^+$ buffer control and the minimum signal was the rPtxS1-catalyzed reaction in the presence of rGαi. The raw fluorescence values were always subtracted from blank containing buffer. The assay was optimized to reach 60% NAD$^+$ consumption. The optimized conditions for the assay are 125 nM rPtxS1, 500 nM NAD$^+$ and 1 µM rGαi. The reaction has incubation time of 40 minutes at 25°C with shaking at 300 rpm. The DMSO concentration used was 0.1%. DMSO tolerance test was done with optimized conditions (0.1-5%). For rGαi substrate-independent NAD$^+$ consumption activity of rPtxS1, identical conditions were used except that rGαi was excluded with longer incubation time of 60 minutes. Statistical analyses on typically 8 parallel values was conducted using two-tailed Student's t-test two sample equal variance. ***ii)* validation of the NAD$^+$ consumption assay** In order to establish repeatability of values for maximum and minimum signals between plates, wells and days, five control plates were tested. Experimental conditions and protein batches used for assay validation were the same. Three plates were made on one day while second and third days had one plate each. Each plate had 40 wells for maximum and minimum signals individually with buffer blanks. The CV% were calculated separately for minimum and maximum signals using (Standard deviation/average) *100. Assay parameters such as signal-to-noise (S/N), (S/B) signal-to-background, screening window coefficient (Z') were calculated as described previously [32, 33]. ***iii) small molecule library screening*** Each plate had buffer blank, control reaction

(minimum signal, with rPtxS1-wt) and maximum signal (NAD^+ and rGαi). Both maximum and minimum signals contain 0.1% DMSO. To correct for inherent fluorescence of compounds separate controls with NAD^+, Gαi and compounds were prepared. Compounds were tested at a concentration of 10 μM. Compounds displaying inhibition more than 50% were considered as hits. Compound library for screening was obtained from the National Cancer Institute (NCI) Developmental Therapeutics program repository (https://dtp.cancer.gov). After the screening, we re-ordered the primary hit compounds in a powder form for subsequent *in vitro* and *in vivo* analyses. The hit compounds were analyzed to identify pan-assay interference compounds or aggregators (zinc15.docking.org). ***iv) IC_{50} measurements*** Assay incubation time was adjusted such that the substrate conversion did not exceed 30% in order to minimize the effect of reduction in substrate concentration while maintaining a robust signal. Compounds were tested from a concentration range of (100-0.01 μM) in half-log dilution series. Each plate had buffer blank, positive control where PtxS1-wt is added which corresponds to 100% activity and negative control (without enzyme) where the activity was 0%. Control values were included as two half-log units below and above the inhibitor concentration series for reactions with 0% and 100% activity. IC_{50} values were obtained by fitting data to log (inhibitor) vs response - variable slope using GraphPad (GraphPad software, Inc.) Chemical structures were drawn using MarvinSketch 5.11.3 (chemAxon) or ChemDraw 18.0 (Perkin-Elmer).

Structure preparation and molecular docking – The 2.7 Å resolution crystal structure of pertussis toxin was accessed from the Protein Data Bank (PDB) (PDB_1BCP [16]). Herein, we considered only the catalytic PtxS1 subunit (1BCP, chain A). Residues 222-269 of PtxS1 were also removed from the coordinate file (see Fig. 1 and 2). The truncated structure was then prepared for docking using the protein preparation wizard [46] in Maestro (Schrödinger Release 2019-1: Maestro,

Schrödinger, LLC, New York, NY, 2019). Hydrogen atoms were added, protonation states of ionizable groups were determined and the structure was energy minimized. A grid outlining the binding pocket was specified based on the superimposition of the PtxS1 structure with the S1 subunit of the pertussis-like toxin structure from *E. coli* with bound NAD^+ (PDB_4Z9D; [31]). The two toxins are 30% identical in primary amino acid sequence. The ligands NSC228155 (7-nitro-4-(1-oxidopyridin-1-ium-2-yl)sulfanyl-2,1,3-benzoxadiazole) and NSC29193 (purine-2,8-dithiol) were prepared for docking using the LigPrep program in Maestro (Schrödinger Release 2019-1: LigPrep, Schrödinger, LLC, New York, NY, 2019). Possible ionization states of the ligands at pH 7.0 ± 2.0 were determined and, in the case of NSC29193, four tautomeric states were also produced. The ligands were docked to the pertussis S1 structure using the glide XP and SP methods [47], keeping the protein structure rigid but allowing ligand flexibility, producing up to 20 poses for each ligand and tautomer. Since the resulting XP docking poses exhibited few interactions, the SP docking results were pursued further. The poses were ranked according to the glide docking score and free energy of binding calculations made with the Prime MM-GBSA module (Schrödinger Release 2019-1: Prime, Schrödinger, LLC, New York, NY, 2019).

Molecular dynamics simulation – Molecular dynamics simulation (MDS) of the selected binding poses of NSC228155 and NSC29193 bound to the S1 structure was used to study the dynamics of the protein-ligand complexes using the Desmond program [48] in Maestro. The complexes were solvated using a TIP3P water model [49] in an octahedral box, with a 10 Å distance between solute surface atoms and an edge of the box. The systems were neutralized by adding Na^+ counterions. Additional Na^+/Cl^- ions were added to bring the systems to a 150 mM salt concentration. The simulations were carried out using the OPLS3e force field [50] at constant temperature (300 K) and

638 constant pressure (1 atm), which were respectively regulated using the Nose-Hoover chain
639 thermostat [51] and Martyna-Tobias-Klein barostat [52]. Short-range and long-range interactions were
640 computed with a 9 Å distance cutoff. The RESPA integrator [53] was employed with a 6.0 fs time
641 step for long-range non-bonded interactions and a 2.0 fs time step for bonded and short range non-
642 bonded interactions. The systems were relaxed with the default equilibration protocol in Desmond,
643 followed by a 100 ns production simulation. Energies were saved every 1.2 ps, whereas coordinates
644 were recorded every 100 ps. The resulting trajectories were analyzed in terms of ligand stability
645 (as root mean squared deviation, RMSD) and lifetime of protein-ligand interactions using the
646 Simulation Interactions Diagram application in Desmond.
647
648 ***In vivo* ADP-ribosylation assay** – HEK293T cells grown in DMEM + 10% FBS were seeded in 3
649 mL volumes in 6-well plates (500 000 cells/well) in the late afternoon. The next morning fresh
650 media containing NSC228155 at concentrations of 0.1, 1 and 5 μM was exchanged to the cells
651 (0.05% DMSO in all reactions, including control reactions). Cells were incubated for 30 minutes
652 at 37°C under normal cell culturing conditions, after which pertussis AB_5 holotoxin (10 or 100
653 ng/mL, List Biological Laboratories Inc., 179A) was added to the cells and incubation was
654 continued for 2 h. Cells were then transferred on ice and washed twice with PBS and collected into
655 70 μL of lysis buffer [50 mM Tris-HCl (pH 7.5), 400 mM NaCl, 0.1% sodium deoxycholate, 1%
656 NP-40, 75 μM tannic acid (PARG inhibitor), 40 μM PJ34 (PARP inhibitor) supplemented with
657 Pierce Protease and Phosphatase Inhibitor Mini Tablets (40 μL/mL of stock solution – one tablet /
658 2 mL H_2O, Thermo Scientific, 88668). Samples were kept on ice for 30 minutes and centrifuged
659 for 15 minutes, 4°C, 16100 × g. Protein concentration was measured from the supernatants with
660 Bradford protein assay. The samples were scaled for protein content to allow loading of 30 μg of

total protein per lane in the SDS-PAGE. Laemmli loading dye was added to 1 × and the samples were boiled for 10 minutes at 95°C. The samples were run on SDS-PAGE and transferred to nitrocellulose membranes, followed by blocking with 4% (w/v) BSA in TBST. Membranes were probed in TBST containing 2% (w/v) BSA for mono-ADP-ribose with rabbit polyclonal anti-mono-ADP-ribose (1:1000) (Hottiger-laboratory), for GAPDH with mouse monoclonal anti-GAPDH (1:1000) (Abcam, ab9484), for Gαi with mouse monoclonal anti-Gαi (1:500) (Santa Cruz Biotechnology, sc-136478), for poly-ADP-ribose with rabbit polyclonal anti-PAR (1:1000) (Enzo Life Sciences, ALX-210-890A), for PtxS1 with mouse monoclonal anti-PtxS1 antibody (10D6) (1:200) (NIBSC, 99/512) and for PARP1 with mouse monoclonal anti-PARP1 (1:300) (Santa Cruz Biotechnology, sc-8007) on a rotary for 24-48 h. Membranes were washed thrice with TBST containing 2% (w/v) BSA for ten minutes each time. Membranes were incubated in TBST containing 2% (w/v) BSA with mouse IgG kappa binding protein conjugated to horseradish peroxidase (1:5000) (sc-516102, Santa Cruz Biotechnology) or goat anti-rabbit IgG conjugated to horseradish peroxidase (1:5000) (sc-2004, Santa Cruz Biotechnology) for 3 h at 4°C on a rotary and washed thrice with TBST for ten minutes each time. Membranes were subsequently developed with WesternBright ECL (Advansta) and imaged on ImageQuant LAS 4000 (GE Healthcare). Pixel intensities were quantified form the Western blot TIFF-files using ImageJ 1.44o (NIH, USA, https://imagej.nih.gov/ij/index.html).

MTT cell viability assay – HEK293T cells grown in DMEM + 10% FBS were seeded in 100 µL volumes in 96-well plates (20 000 cells/well) in the late afternoon. The next morning fresh media containing varying concentrations (0, 0.1, 0.5, 1, 2.5, 5, 10, 20, 40, 60 µM) of NSC228155 was added in triplicate. In all the wells final concentration of DMSO was 0.6%. Cells were incubated

for 2.5 h at 37°C under normal cell culturing conditions. Cell viability was investigated using the CellTiter 96 Non-Radioactive Cell Proliferation Assay (MTT) (Promega, G4002) according to the manufacturer's instructions. Incubation time with the MTT dye solution was 1 h at 37°C under normal cell culturing conditions. NSC228155 cytotoxicity IC_{50} value was calculated using GraphPad (GraphPad software, Inc.) Data are displayed as means and the standard error of the mean. Data were normalized to cells treated with 0.6% DMSO (negative controls, 100% viability) and cells killed with 200 µM H_2O_2 (positive control, 0% viability) and expressed as percentage of these controls. Normalized response is compared to common log of the inhibitor concentration (µM) and the IC_{50} calculated using a variable slope. Statistical analyses were conducted using two-tailed Student's t-test two sample equal variance.

Microscopy – HEK293T cells were seeded on collagen-coated (50 µg/ml, Gibco, A1048301) glass coverslips in 24-wells in DMEM + 10% FBS (100 000/well) in the late afternoon and incubated overnight at 37 °C. The next morning fresh media containing NSC228155 at concentration of 5 µM was exchanged to the cells (0.05% DMSO in all reactions, including control reactions). Cells were incubated for 30 minutes at 37 °C under normal cell culturing conditions, after which Alexa Fluor 594-conjugated Cholera Toxin Subunit B (Thermo Fisher Scientific, C34777) was added to cells at concentration of 1 µg/ml and incubation was continued for 2 h. Cells were fixed with 4% paraformaldehyde (PFA) in PBS for 10 minutes at room temperature, washed three times with PBS and permeabilized with 0.1% Triton X-100 in PBS for 5 min at room temperature followed by a single wash with PBS. DNA was stained with DAPI (300 nM) (Santa Cruz Biotechnology, sc-3598) for 5 minutes at room temperature. After washing the cells three times in PBS, coverslips were mounted onto microscope slides with MOWIOL 4-88 (Sigma, 475904) containing 2.5% 1,4-diazobicyclo[2,2,2]-octane (DABCO) antifade (Sigma, 8.03456). The cells were imaged with a

Zeiss AxioImager M1 microscope and a Zeiss AxioCam MRm monochrome camera using a EC Plan-Neofluar 40x/1.30 Oil M27 objective, driven by Zen 2 pro software.

ANCILLARY INFORMATION

Description of the Supporting Information:

Figure S1. SEC-analysis of rPtxS1-rGαi complex formation in solution.

Figure S2. Catalytic activity of rPtxS1 is dependent on two acidic amino acids.

Figure S3. rPtxS1 is incapable of ADP-ribosylating a C351A-mutant of rGαi.

Figure S4. Molecular dynamics simulation data.

Figure S5. Prediction of binding poses of NSC228155 and NSC29193 to PtxS1.

Figure S6. Effect of NSC228155 on the amount of cell associated PtxS1 and the proteolytic processing of PtxS1.

Figure S7. Effect of NSC228155 on the retrograde endosomal trafficking.

CORRESPONDING AUTHOR INFORMATION

Arto Pulliainen, Ph.D.

Institute of Biomedicine, Research Center for Cancer, Infections, and Immunity, University of Turku, Kiinamyllynkatu 10, FI-20520, Turku, Finland

Phone: +358-40-1586044, Fax: not available, E-mail: arto.pulliainen@utu.fi

Dr. Lari Lehtiö, Ph.D.

Faculty of Biochemistry and Molecular Medicine & Biocenter Oulu, University of Oulu, Aapistie 7 B, FI-90220, Oulu, Finland

Phone: +358-2-9448 1169, Fax: not available, E-mail: lari.lehtio@oulu.fi

AUTHOR CONTRIBUTIONS

Yashwanth Ashok and Moona Miettinen contributed equally to this study.

ACKNOWLEDGEMENTS

The research in the laboratory of A.T.P. is financially supported by Academy of Finland (grant no. 295296), Sigrid Juselius Foundation, Turku Doctoral Programme of Molecular Medicine (TuDMM) (to M.M.) and University of Turku, Turku, Finland. This work was funded in the L.L. laboratory by Academy of Finland (grant no. 287063, 294085 and 319299). The use of the facilities of the Biocenter Oulu for DNA sequencing, Proteomics and Protein Analysis and Protein Crystallography, a member of Biocenter Finland and Instruct-FI, are gratefully acknowledged. The laboratory of M.S.J. is supported by Sigrid Juselius Foundation, Joe, Pentti and Tor Memorial Fund, and Doctoral Network of Informational and Structural Biology (to M.T., Åbo Akademi Graduate School); computational infrastructure and core faculty support from Biocenter Finland (bioinformatics, structural biology and drug discovery and chemical biology nodes), CSC IT Center for Science; Academy of Finland FIRI infrastructure funding (grant no. 320005); screening core faculty of Biocity Turku, and Drug Discovery and Diagnostics strategic funding to Åbo Akademi University. We thank Dr. Jukka Lehtonen for his scientific IT support. The funders had no role in study design, data collection and interpretation, or the decision to submit the work for publication. The authors declare that they have no conflicts of interest.

ABBREVIATIONS

ART	ADP-ribosyltransferase
ADP	adenosine diphosphate
B. pertussis	*Bordetella pertussis*
BSA	bovine serum albumin
DMSO	dimethyl sulfoxide
DSF	differential scanning fluorimetry
E. coli	*Escherichia coli*
Gαi	inhibitory α-subunit of heterotrimeric G-protein
GPCR	G-protein coupled receptor
HRP	horse radish peroxidase
IC_{50}	half maximal inhibitory concentration
LB	Luria-Bertani
MALS	multi-angle light scattering
MAR	mono-ADP-ribose
MDS	molecular dynamic simulation
NAD^+	nicotinamide adenine dinucleotide
PAR	poly-ADP-ribose
PARP1	poly(ADP-ribose) polymerase 1 (also known as ARTD1)
PCR	polymerase chain reaction
PDB	protein data bank
PtxS1	pertussis toxin S1 subunit
rGαi	recombinant inhibitory α-subunit of heterotrimeric G-protein
RMSD	root-mean-square deviation
rPtxS1	recombinant pertussis toxin S1 subunit
SDS-PAGE	sodium dodecyl sulphate polyacrylamide gel electrophoresis
SEC	size exclusion chromatography
TBST	Tris-buffered saline containing 0.05 % Tween
Tm	melting temperature

REFERENCES

1. Kilgore, P. E.; Salim, A. M.; Zervos, M. J.; Schmitt, H. J., Pertussis: microbiology, disease, treatment, and prevention. *Clin Microbiol Rev* **2016,** *29* (3), 449-86. DOI: 10.1128/CMR.00083-15.

2. Yeung, K. H. T.; Duclos, P.; Nelson, E. A. S.; Hutubessy, R. C. W., An update of the global burden of pertussis in children younger than 5 years: a modelling study. *Lancet Infect Dis* **2017,** *17* (9), 974-980. DOI: 10.1016/S1473-3099(17)30390-0.

3. Skoff, T. H.; Baumbach, J.; Cieslak, P. R., Tracking pertussis and evaluating control measures through enhanced pertussis surveillance, Emerging Infections Program, United States. *Emerg Infect Dis* **2015,** *21* (9), 1568-73. DOI: 10.3201/eid2109.150023.

4. Guillot, S.; Descours, G.; Gillet, Y.; Etienne, J.; Floret, D.; Guiso, N., Macrolide-resistant *Bordetella pertussis* infection in newborn girl, France. *Emerg Infect Dis* **2012,** *18* (6), 966-8. DOI: 10.3201/eid1806.120091.

5. Wang, Z.; Li, Y.; Hou, T.; Liu, X.; Liu, Y.; Yu, T.; Chen, Z.; Gao, Y.; Li, H.; He, Q., Appearance of macrolide-resistant *Bordetella pertussis* strains in China. *Antimicrob Agents Chemother* **2013,** *57* (10), 5193-4. DOI: 10.1128/AAC.01081-13.

6. Warfel, J. M.; Zimmerman, L. I.; Merkel, T. J., Acellular pertussis vaccines protect against disease but fail to prevent infection and transmission in a nonhuman primate model. *Proc Natl Acad Sci U S A* **2014,** *111* (2), 787-92. DOI: 10.1073/pnas.1314688110.

7. Scanlon, K.; Skerry, C.; Carbonetti, N., Association of pertussis toxin with severe pertussis disease. *Toxins (Basel)* **2019,** *11* (7). DOI: 10.3390/toxins11070373.

8. Bouchez, V.; Brun, D.; Cantinelli, T.; Dore, G.; Njamkepo, E.; Guiso, N., First report and detailed characterization of *B. pertussis* isolates not expressing pertussis toxin or pertactin. *Vaccine* **2009,** *27* (43), 6034-41. DOI: 10.1016/j.vaccine.2009.07.074.

9. Morse, S. I.; Morse, J. H., Isolation and properties of the leukocytosis- and lymphocytosis-promoting factor of *Bordetella pertussis*. *J Exp Med* **1976,** *143* (6), 1483-502.

10. Hall, E.; Parton, R.; Wardlaw, A. C., Cough production, leucocytosis and serology of rats infected intrabronchially with *Bordetella pertussis*. *J Med Microbiol* **1994,** *40* (3), 205-13. DOI: 10.1099/00222615-40-3-205.

11. Parton, R.; Hall, E.; Wardlaw, A. C., Responses to *Bordetella pertussis* mutant strains and to vaccination in the coughing rat model of pertussis. *J Med Microbiol* **1994,** *40* (5), 307-12. DOI: 10.1099/00222615-40-5-307.

12. Scanlon, K. M.; Snyder, Y. G.; Skerry, C.; Carbonetti, N. H., Fatal pertussis in the neonatal mouse model is associated with pertussis toxin-mediated pathology beyond the airways. *Infect Immun* **2017,** *85* (11). DOI: 10.1128/IAI.00355-17.

13. Stein, P. E.; Boodhoo, A.; Armstrong, G. D.; Cockle, S. A.; Klein, M. H.; Read, R. J., The crystal structure of pertussis toxin. *Structure* **1994,** *2* (1), 45-57.

14. Stein, P. E.; Boodhoo, A.; Armstrong, G. D.; Heerze, L. D.; Cockle, S. A.; Klein, M. H.; Read, R. J., Structure of a pertussis toxin-sugar complex as a model for receptor binding. *Nat Struct Biol* **1994,** *1* (9), 591-6.

15. Weiss, A. A.; Johnson, F. D.; Burns, D. L., Molecular characterization of an operon required for pertussis toxin secretion. *Proc Natl Acad Sci U S A* **1993,** *90* (7), 2970-4.

16. Hazes, B.; Boodhoo, A.; Cockle, S. A.; Read, R. J., Crystal structure of the pertussis toxin-ATP complex: a molecular sensor. *J Mol Biol* **1996,** *258* (4), 661-71. DOI: 10.1006/jmbi.1996.0277.

17. Simon, N. C.; Aktories, K.; Barbieri, J. T., Novel bacterial ADP-ribosylating toxins: structure and function. *Nat Rev Microbiol* **2014,** *12* (9), 599-611. DOI: 10.1038/nrmicro3310.

18. Katada, T.; Ui, M., Direct modification of the membrane adenylate cyclase system by islet-activating protein due to ADP-ribosylation of a membrane protein. *Proc Natl Acad Sci U S A* **1982,** *79* (10), 3129-33.

19. West, R. E.; Moss, J.; Vaughan, M.; Liu, T.; Liu, T. Y., Pertussis toxin-catalyzed ADP-ribosylation of transducin. Cysteine 347 is the ADP-ribose acceptor site. *J Biol Chem* **1985,** *260* (27), 14428-30.

20. Graf, R.; Codina, J.; Birnbaumer, L., Peptide inhibitors of ADP-ribosylation by pertussis toxin are substrates with affinities comparable to those of the trimeric GTP-binding proteins. *Mol Pharmacol* **1992,** *42* (5), 760-4.

21. Weis, W. I.; Kobilka, B. K., The molecular basis of G protein-soupled seceptor activation. *Annu Rev Biochem* **2018,** *87*, 897-919. DOI: 10.1146/annurev-biochem-060614-033910.

22. Eby, J. C.; Hoffman, C. L.; Gonyar, L. A.; Hewlett, E. L., Review of the neutrophil response to *Bordetella pertussis* infection. *Pathog Dis* **2015,** *73* (9), ftv081. DOI: 10.1093/femspd/ftv081.

23. Turgeon, Z.; Jørgensen, R.; Visschedyk, D.; Edwards, P. R.; Legree, S.; McGregor, C.; Fieldhouse, R. J.; Mangroo, D.; Schapira, M.; Merrill, A. R., Newly discovered and characterized antivirulence compounds inhibit bacterial mono-ADP-ribosyltransferase toxins. *Antimicrob Agents Chemother* **2011,** *55* (3), 983-91. DOI: 10.1128/AAC.01164-10.

24. Jørgensen, R.; Purdy, A. E.; Fieldhouse, R. J.; Kimber, M. S.; Bartlett, D. H.; Merrill, A. R., Cholix toxin, a novel ADP-ribosylating factor from *Vibrio cholera*e. *J Biol Chem* **2008,** *283* (16), 10671-8. DOI: 10.1074/jbc.M710008200.

25. Pinto, A. F.; Ebrahimi, M.; Saleeb, M.; Forsberg, Å.; Elofsson, M.; Schüler, H., Identification of Inhibitors of *Pseudomonas aeruginosa* Exotoxin-S ADP-Ribosyltransferase Activity. *J Biomol Screen* **2016,** *21* (6), 590-5. DOI: 10.1177/1087057116629923.

852 26. Maurer, B.; Mathias, U.; Papatheodorou, P.; Shekfeh, S.; Orth, J.; Jank, T.; Schwan, C.;
853 Sippl, W.; Aktories, K.; Jung, M., From cosubstrate similarity to inhibitor diversity--inhibitors of
854 ADP-ribosyltransferases from kinase inhibitor screening. *Mol Biosyst* **2011,** *7* (3), 799-808. DOI:
855 10.1039/c0mb00151a.
856 27. Zhang, G., Design, synthesis, and evaluation of bisubstrate analog inhibitors of cholera
857 toxin. *Bioorg Med Chem Lett* **2008,** *18* (13), 3724-7. DOI: 10.1016/j.bmcl.2008.05.049.
858 28. Lugo, M. R.; Merrill, A. R., A comparative structure-function analysis of active-site
859 inhibitors of *Vibrio cholerae* cholix toxin. *J Mol Recognit* **2015,** *28* (9), 539-52. DOI:
860 10.1002/jmr.2469.
861 29. Cortina, G.; Krueger, K. M.; Barbieri, J. T., The carboxyl terminus of the S1 subunit of
862 pertussis toxin confers high affinity binding to transducin. *J Biol Chem* **1991,** *266* (35), 23810-4.
863 30. Locht, C.; Cieplak, W.; Marchitto, K. S.; Sato, H.; Keith, J. M., Activities of complete and
864 truncated forms of pertussis toxin subunits S1 and S2 synthesized by *Escherichia coli*. *Infect*
865 *Immun* **1987,** *55* (11), 2546-53.
866 31. Littler, D. R.; Ang, S. Y.; Moriel, D. G.; Kocan, M.; Kleifeld, O.; Johnson, M. D.; Tran, M.
867 T.; Paton, A. W.; Paton, J. C.; Summers, R. J.; Schembri, M. A.; Rossjohn, J.; Beddoe, T.,
868 Structure-function analyses of a pertussis-like toxin from pathogenic *Escherichia coli* reveal a
869 distinct mechanism of inhibition of trimeric G-proteins. *J Biol Chem* **2017,** *292* (36), 15143-15158.
870 DOI: 10.1074/jbc.M117.796094.
871 32. Putt, K. S.; Hergenrother, P. J., An enzymatic assay for poly(ADP-ribose) polymerase-1
872 (PARP-1) via the chemical quantitation of NAD(+): application to the high-throughput screening
873 of small molecules as potential inhibitors. *Anal Biochem* **2004,** *326* (1), 78-86. DOI:
874 10.1016/j.ab.2003.11.015.

875 33. Venkannagari, H.; Fallarero, A.; Feijs, K. L.; Lüscher, B.; Lehtiö, L., Activity-based assay
876 for human mono-ADP-ribosyltransferases ARTD7/PARP15 and ARTD10/PARP10 aimed at
877 screening and profiling inhibitors. *Eur J Pharm Sci* **2013,** *49* (2), 148-56. DOI:
878 10.1016/j.ejps.2013.02.012.
879 34. Narwal, M.; Fallarero, A.; Vuorela, P.; Lehtiö, L., Homogeneous screening assay for human
880 tankyrase. *J Biomol Screen* **2012,** *17* (5), 593-604. DOI: 10.1177/1087057112436558.
881 35. Finck-Barbançon, V.; Barbieri, J. T., Preferential processing of the S1 subunit of pertussis
882 toxin that is bound to eukaryotic cells. *Mol Microbiol* **1996,** *22* (1), 87-95.
883 36. Pizza, M.; Covacci, A.; Bartoloni, A.; Perugini, M.; Nencioni, L.; De Magistris, M. T.;
884 Villa, L.; Nucci, D.; Manetti, R.; Bugnoli, M., Mutants of pertussis toxin suitable for vaccine
885 development. *Science* **1989,** *246* (4929), 497-500.
886 37. Locht, C.; Keith, J. M., Pertussis toxin gene: nucleotide sequence and genetic organization.
887 *Science* **1986,** *232* (4755), 1258-64.
888 38. Nicosia, A.; Perugini, M.; Franzini, C.; Casagli, M. C.; Borri, M. G.; Antoni, G.; Almoni,
889 M.; Neri, P.; Ratti, G.; Rappuoli, R., Cloning and sequencing of the pertussis toxin genes: operon
890 structure and gene duplication. *Proc Natl Acad Sci U S A* **1986,** *83* (13), 4631-5.
891 39. Moss, J.; Stanley, S. J.; Burns, D. L.; Hsia, J. A.; Yost, D. A.; Myers, G. A.; Hewlett, E. L.,
892 Activation by thiol of the latent NAD glycohydrolase and ADP-ribosyltransferase activities of
893 Bordetella pertussis toxin (islet-activating protein). *J Biol Chem* **1983,** *258* (19), 11879-82.
894 40. Sakanyan, V.; Hulin, P.; Alves de Sousa, R.; Silva, V. A.; Hambardzumyan, A.; Nedellec,
895 S.; Tomasoni, C.; Logé, C.; Pineau, C.; Roussakis, C.; Fleury, F.; Artaud, I., Activation of EGFR
896 by small compounds through coupling the generation of hydrogen peroxide to stable dimerization
897 of Cu/Zn SOD1. *Sci Rep* **2016,** *6*, 21088. DOI: 10.1038/srep21088.

41. Miettinen, M.; Vedantham, M.; Pulliainen, A. T., Host poly(ADP-ribose) polymerases (PARPs) in acute and chronic bacterial infections. *Microbes Infect* **2019,** *21* (10), 423-431. DOI: 10.1016/j.micinf.2019.06.002.

42. Winter, K.; Zipprich, J.; Harriman, K.; Murray, E. L.; Gornbein, J.; Hammer, S. J.; Yeganeh, N.; Adachi, K.; Cherry, J. D., Risk factors associated with infant deaths from pertussis: a case-control study. *Clin Infect Dis* **2015,** *61* (7), 1099-106. DOI: 10.1093/cid/civ472.

43. Acquaye-Seedah, E.; Huang, Y.; Sutherland, J. N.; DiVenere, A. M.; Maynard, J. A., Humanised monoclonal antibodies neutralise pertussis toxin by receptor blockade and reduced retrograde trafficking. *Cell Microbiol* **2018,** *20* (12), e12948. DOI: 10.1111/cmi.12948.

44. Nguyen, A. W.; Wagner, E. K.; Laber, J. R.; Goodfield, L. L.; Smallridge, W. E.; Harvill, E. T.; Papin, J. F.; Wolf, R. F.; Padlan, E. A.; Bristol, A.; Kaleko, M.; Maynard, J. A., A cocktail of humanized anti-pertussis toxin antibodies limits disease in murine and baboon models of whooping cough. *Sci Transl Med* **2015,** *7* (316), 316ra195. DOI: 10.1126/scitranslmed.aad0966.

45. Pulliainen, A. T.; Pieles, K.; Brand, C. S.; Hauert, B.; Böhm, A.; Quebatte, M.; Wepf, A.; Gstaiger, M.; Aebersold, R.; Dessauer, C. W.; Dehio, C., Bacterial effector binds host cell adenylyl cyclase to potentiate Gαs-dependent cAMP production. *Proc Natl Acad Sci U S A* **2012,** *109* (24), 9581-6. DOI: 10.1073/pnas.1117651109.

46. Sastry, G. M.; Adzhigirey, M.; Day, T.; Annabhimoju, R.; Sherman, W., Protein and ligand preparation: parameters, protocols, and influence on virtual screening enrichments. J *Comput Aided Mol Des* **2013,** *27* (3), 221-34. DOI: 10.1007/s10822-013-9644-8.

47. Friesner, R. A.; Banks, J. L.; Murphy, R. B.; Halgren, T. A.; Klicic, J. J.; Mainz, D. T.; Repasky, M. P.; Knoll, E. H.; Shelley, M.; Perry, J. K.; Shaw, D. E.; Francis, P.; Shenkin, P. S., Glide: a new approach for rapid, accurate docking and scoring. 1. Method and assessment of docking accuracy. J *Med Chem* **2004,** *47* (7), 1739-49. DOI: 10.1021/jm0306430.

48. Bowers, K. J.; Chow, E.; Xu, H.; Dror, R. O.; Eastwood, M. P.; Gregersen, B. A.; Klepeis, J. L.; Kolossvary, I.; Moraes, M. A.; Sacerdoti, F. D.; Salmon, J. o. K.; Shan, Y.; Shaw, D. E., Scalable algorithms for molecular dynamics simulations on commodity clusters. *Proceedings of ACM/IEEE Conference on Supercomputing (SC06) Tampa Florida* 2006, November 11-17.

49. Jorgensen, W. L.; Chandrasekhar, J.; Madura, J. D.; Impey, R. W.; Klein, M., Comparison of simple potential functions for simulating liquid water. *J Chem Phys* **1983,** 79:926-35.

50. Harder, E.; Damm, W.; Maple, J.; Wu, C.; Reboul, M.; Xiang, J. Y.; Wang, L.; Lupyan, D.; Dahlgren, M. K.; Knight, J. L.; Kaus, J. W.; Cerutti, D. S.; Krilov, G.; Jorgensen, W. L.; Abel, R.; Friesner, R. A., OPLS3: A Force Field Providing Broad Coverage of Drug-like Small Molecules and Proteins. J *Chem Theory Comput* **2016,** 1*2* (1), 281-96. DOI: 10.1021/acs.jctc.5b00864.

51. Martyna, G. J.; Klein, M. L.; Tuckerman, M., Nose-Hoover chains - the canonical ensemble via continuous dynamics. *J Chem Phys* **1992,** 97:2635-43.

52. Martyna, G. J.; Tobias, D. J.; Klein, M. L., Constant-pressure molecular dynamics algorithms. *J Chem Phys* **1994,** 101:4177-89.

53. Tuckerman, M.; Berne, B. J.; Martyna, G. J., Reversible multiple time scale molecular dynamics. *J Chem Phys* **1992,** 97:1990-2001.

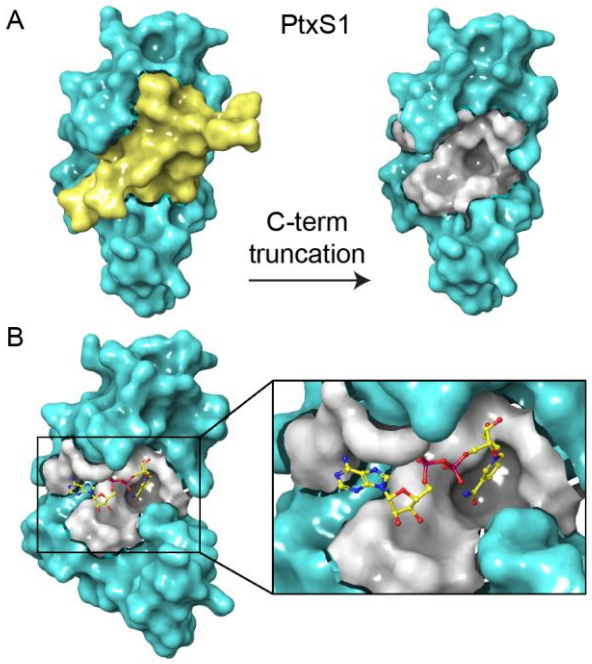

Figure 1. PtxS1 of pertussis toxin. A) Surface representation of the crystal structure of PtxS1 (PDB_1BCP). The truncated C-terminal fragment and the truncation-uncovered ART active site are shown in yellow and grey, respectively. **B)** Possible binding mode of NAD^+ to PtxS1 derived by superimposing the PtxS1 crystal structure (PDB_1BCP) to the crystal structure of active site mutant of pertussis-like toxin from *E. coli* with bound NAD^+ (PDB_4Z9D). Color-coding of atoms in NAD^+: yellow, carbon; blue, nitrogen; red, oxygen; magenta, phosphorus.

941

942

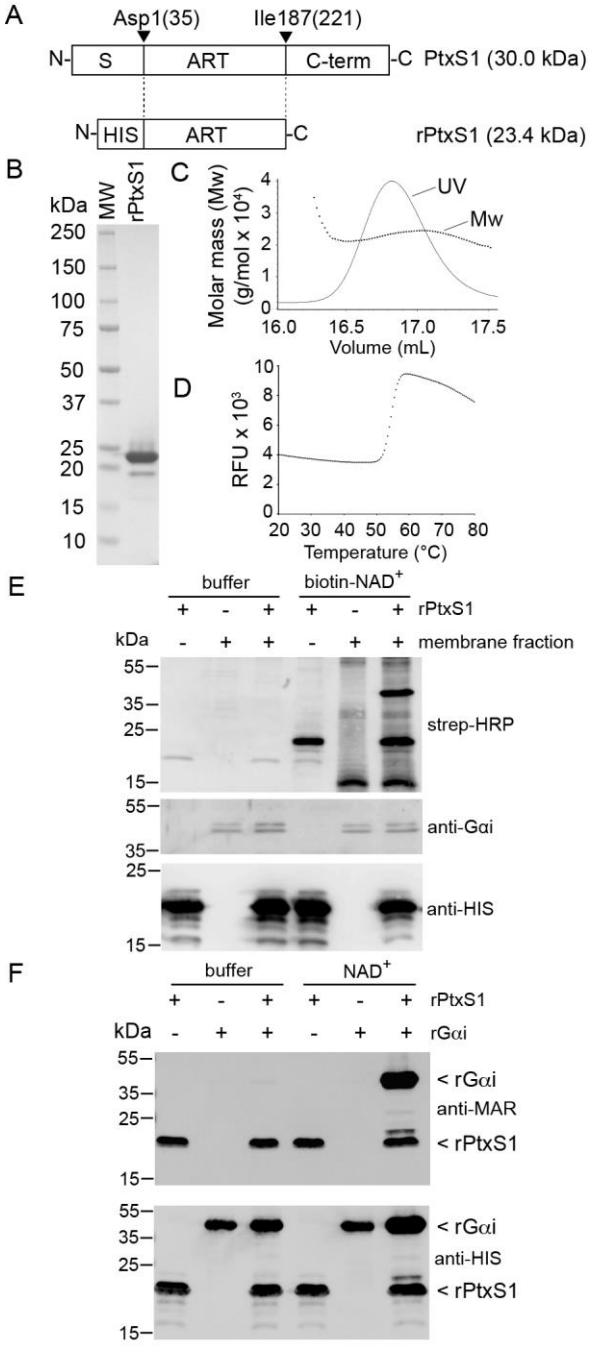

Figure 2. Catalytic activity of rPtxS1. A) Construct design. rPtxS1 lacks the N-terminal secretion signal (S) as well as part of the C-terminus (C-term). N-terminus of the mature PtxS1 starting with Asp35 is classically numbered as the first amino acid of PtxS1. **B)** PageBlue-stained SDS-PAGE gel of SEC-purified rPtxS1. **C)** Representative SEC-MALS result of SEC-purified rPtxS1. **D)** Representative DSF result of SEC-purified rPtxS1. **E)** *In vitro* ADP-ribosylation assay (enzyme-excess condition) for rPtxS1 with NAD⁺-biotin and HEK293T membrane fraction with endogenous level of Gαi. Protein-conjugated ADP-ribose-biotin is detected with streptavidin-HRP. **F)** *In vitro* ADP-ribosylation assay (enzyme-excess condition) for rPtxS1 with NAD⁺ and recombinant N-terminally HIS-tagged Gαi. Protein-conjugated ADP-ribose is detected with a rabbit polyclonal antibody specific for mono-ADP-ribose. Same samples were analyzed in three (Fig. 2E) and two (Fig. 2F) parallel membranes, respectively.

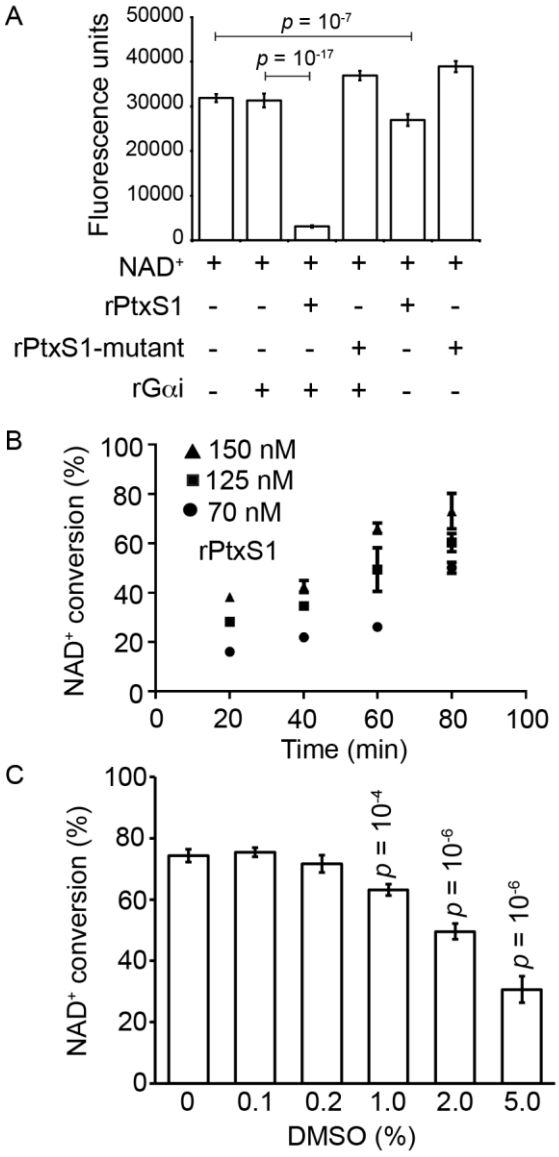

Figure 3. Multiwell fluorometric NAD⁺ quantitation assay. Decrease in fluorescence over time is a measure of NAD⁺-consuming enzymatic activity. **A)** rPtxS1 and rPtxS1-mutant were incubated for 40 min in the presence or for 60 min in the absence of rGαi substrate. **B)** Time and concentration dependency of NAD⁺-consuming enzymatic activity of rPtxS1 in the presence of rGαi substrate. **C)** Effect of DMSO on NAD⁺-consuming enzymatic activity of rPtxS1 in the presence of rGαi substrate. Statistics by two-tailed Student's t-test two sample equal variance.

945

946

947

948

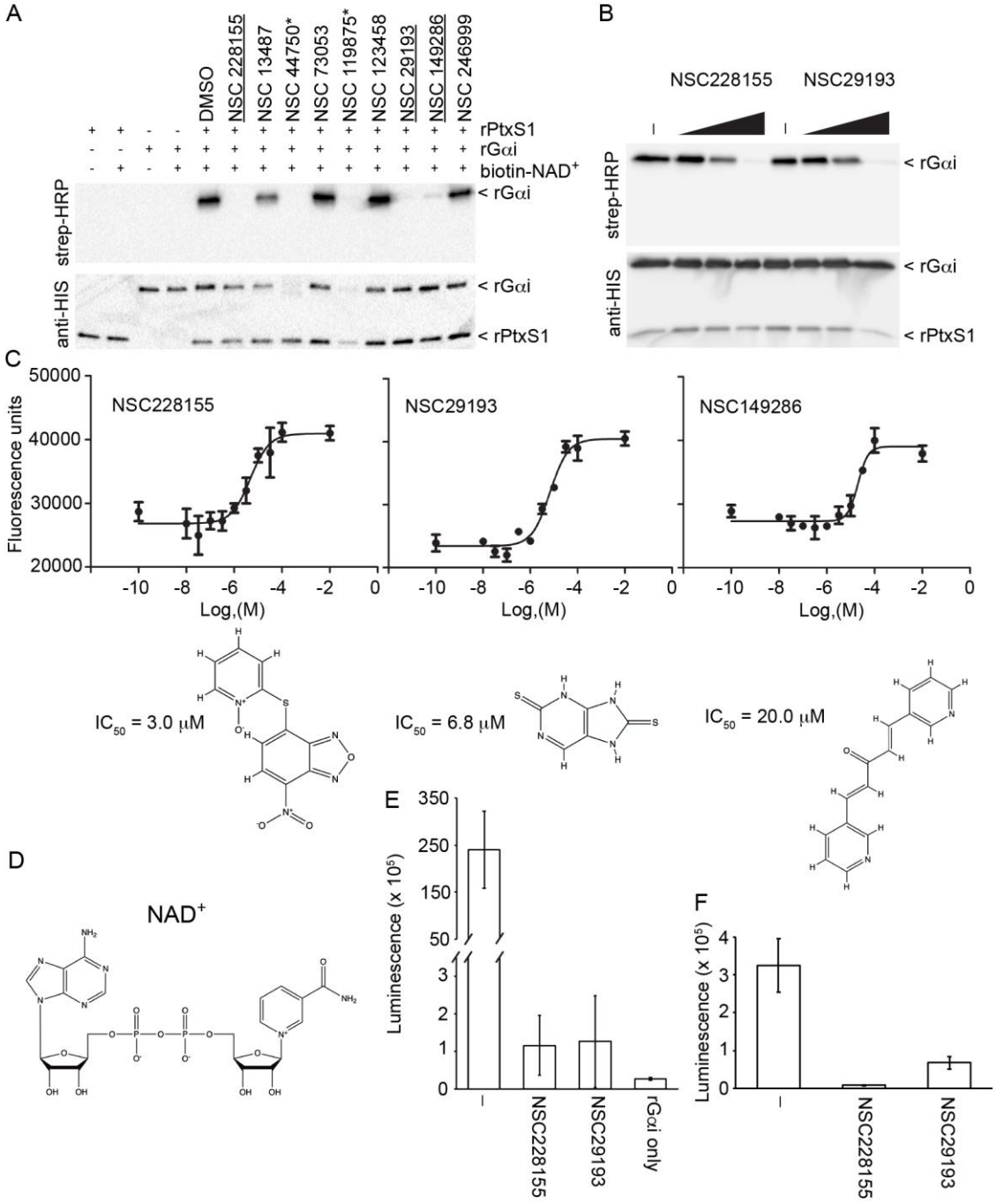

Figure 4. Evaluation of primary compound hits from rPtxS1 inhibitor screen. A) *In vitro* ADP-ribosylation assay (substrate-excess condition) for rPtxS1 (50 nM) with NAD$^+$-biotin (1 μM) and rGαi (500 nM). Protein-conjugated biotin-ADP-ribose was detected with streptavidin-HRP. Compounds (10 μM) marked with an asterisk affect rPtxS1 and/or rGαi protein integrity, and were therefore excluded from further studies. Same samples were analyzed in two parallel membranes. **B)** *In vitro* ADP-ribosylation assay (substrate-excess condition) for rPtxS1 (50 nM) with NAD$^+$-biotin (1 μM), rGαi (500 nM) and compounds (0.1, 1 or 10 μM). Same samples were analyzed in two parallel membranes **C)** IC_{50}-curves and chemical structures of the hit compounds selected based on Fig. 4A data. **D)** Chemical structure of NAD$^+$. **E-F)** *In vitro* ADP-ribosylation assay in a 96-well nickel-coated plate format. Protein-conjugated biotin-ADP-ribose (E: rPtxS1 + rGαi or rGαi only reaction conditions; F; rPtxS1 only reaction condition) was detected with streptavidin-HRP. Reaction compound concentrations were rPtxS1 (500 nM), NAD$^+$-biotin (0.5 μM), rGαi (2 μM) and compounds (200 μM).

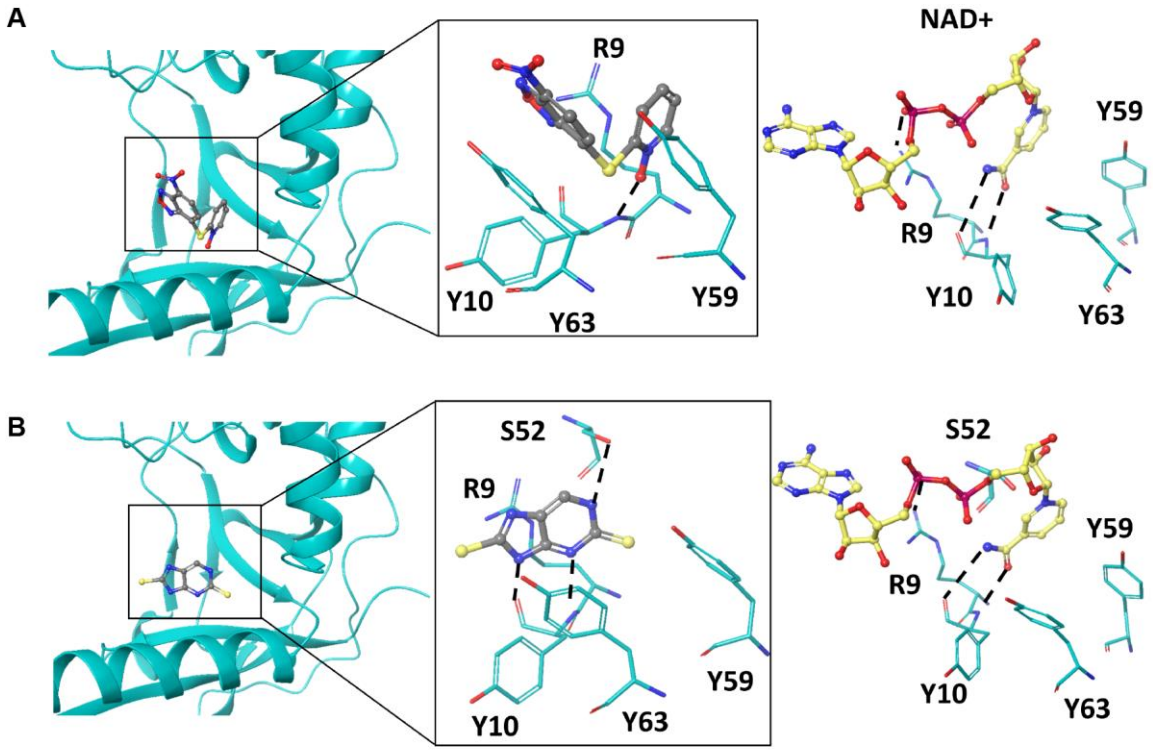

Figure 5. Prediction of binding poses of NSC228155 and NSC29193 to PtxS1. Binding pose 1 of NSC228155 **(A)** and binding pose 1 of NSC29193 **(B)** to PtxS1 (PDB_1BCP, chain A). Residues involved in ligand interactions (sticks) and hydrogen bonds (dotted lines) are shown. Binding mode of NAD^+ to PtxS1 in the corresponding area of the NAD^+-binding pocket is shown in each panel on the right (see also Fig. 1). Color-coding of atoms in NAD^+: yellow, carbon; blue, nitrogen; red, oxygen; magenta, phosphorus.

952

953

954

955

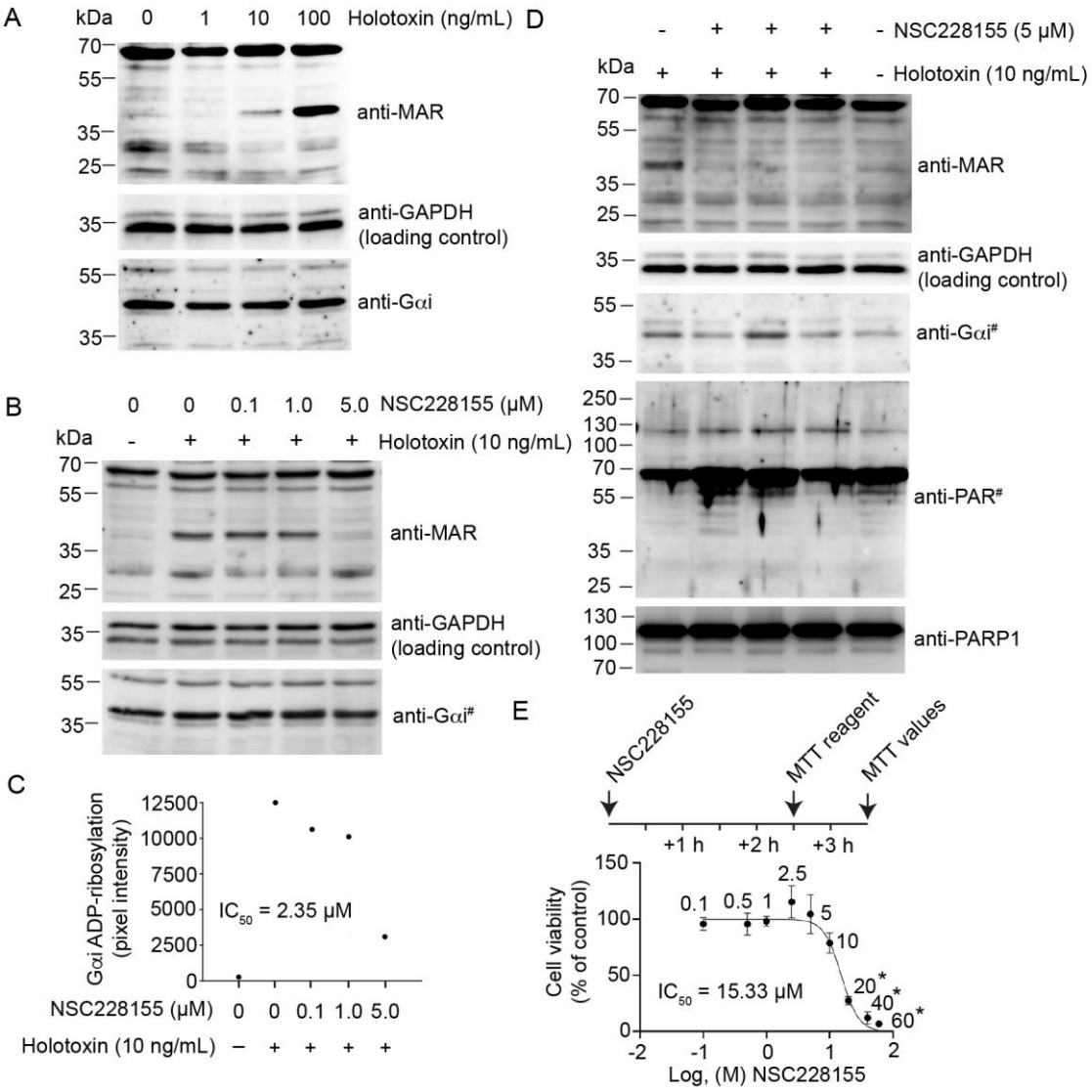

Figure 6. Evaluation of NSC228155 as an inhibitor of pertussis toxin in living human cells. A) Effect of pertussis holotoxin titration on mono-ADP-ribosylation of Gαi in living HEK293T cells (2 h incubation). Protein-conjugated ADP-ribose is detected with a rabbit polyclonal antibody specific for mono-ADP-ribose (MAR). **B)** Effect of NSC228155 titration on pertussis toxin-catalyzed mono-ADP-ribosylation of Gαi in living HEK293T cells. Inhibitors were added 30 min before starting the 2 h holotoxin incubation. #Western blot of a parallel membrane with the same Fig. 6B samples, otherwise Fig. 6A and Fig. 6B blots probed, stripped and re-probed in the order of 1) anti-MAR, 2) anti-GAPDH and 3) anti-Gαi. **C)** Quantitation of the inhibitory effect of NSC228155 on pertussis holotoxin-catalyzed mono-ADP-ribosylation of Gαi. Pixel intensities of the anti-MAR signal (Fig. 6B) were normalized based on the anti-GAPDH loading control. **D)** Effect of 5 μM NSC228155 (triplicate treatment) on pertussis holotoxin-catalyzed mono-ADP-ribosylation of Gαi and cell viability as assessed by the DNA damage-associated auto-poly-ADP-ribosylation of PARP1 and apoptosis-associated PARP1 proteolytic processing. #Western blot of a parallel membrane with the same Fig. 6D samples, otherwise Fig. 6D blots probed, stripped and re-probed in the order of 1) anti-MAR, 2) anti-GAPDH and 3) anti-PARP1. **E)** Effect of NSC228155 titration on metabolic activity of HEK293T cells as analyzed by the MTT-assay 3.5 h after compound addition. Statistics by two-tailed Student's t-test two sample equal variance (*p-value <0.05).

Discovery of compounds inhibiting the ADP-ribosyltransferase activity of pertussis toxin

Yashwanth Ashok[a,#], Moona Miettinen[b,c,#], Danilo Kimio Hirabae de Oliveira[a], Mahlet Z. Tamirat[d], Katja Näreoja[b], Avlokita Tiwari[b], Michael O. Hottiger[e], Mark S. Johnson[d], Lari Lehtiö[a,*] & Arto T. Pulliainen[b,*]

[a]Faculty of Biochemistry and Molecular Medicine, Biocenter Oulu, University of Oulu, Aapistie 7A, P.O. Box 5400, FI-90014, Oulu, Finland

[b]Institute of Biomedicine, Research Center for Cancer, Infections, and Immunity, University of Turku, Kiinamyllynkatu 10, FI-20520, Turku, Finland

[c]Turku Doctoral Programme of Molecular Medicine (TuDMM), University of Turku, Turku, Finland

[d]Structural Bioinformatics Laboratory, Biochemistry, Faculty of Science and Engineering, Åbo Akademi University, Tykistökatu 6A, FI-20520, Turku, Finland

[e]Department of Molecular Mechanisms of Disease, University of Zurich, Winterthurerstrasse 190, 8057, Zurich, Switzerland

[#] Equal contribution

[*] Corresponding authors (Lari.Lehtio@oulu.fi, arto.pulliainen@utu.fi)

Supporting Information – Figures S1-S7, Table S1-S2

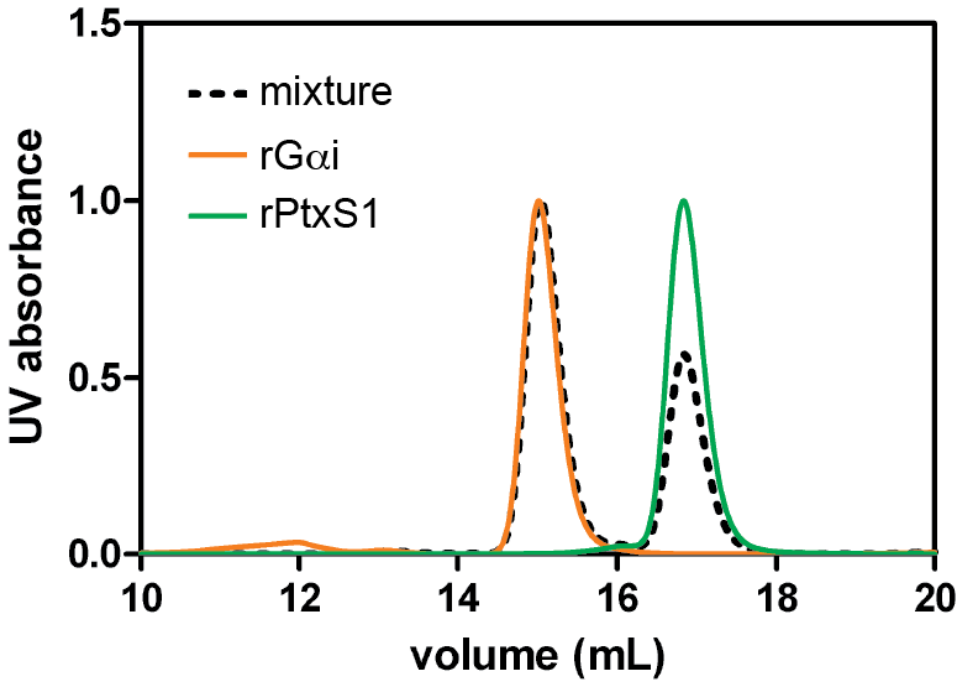

Figure S1. SEC-analysis of rPtxS1-rGαi complex formation in solution. Proteins were injected into the column either alone (100 µg) or in a mixture (100 µg + 100 µg).

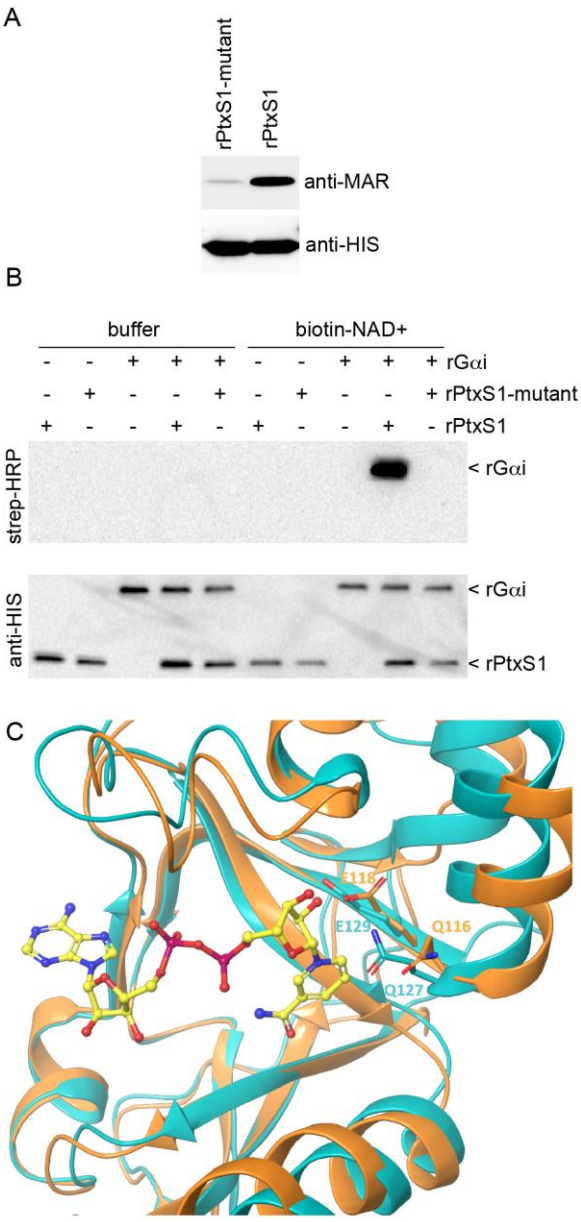

Figure S2. Catalytic activity of rPtxS1 is dependent on two acidic amino acids. A) Effect of Q127D/E129D mutation to auto-ADP-ribosylation of rPtxS1 that took place inside the *E. coli* expression host. **B)** Effect of Q127D/E129D mutation to rPtxS1-catalyzed ADP-ribosylation of rGαi *in vitro* (substrate-excess conditions). Blots probed, stripped and re-probed in the order of 1) strep-HRP and 2) anti-HIS. **C)** Structural comparison of the NAD^+-binding pocket of pertussis-like toxin from *E. coli* (PDB_4Z9C, PDB_4Z9D) with the corresponding area of PtxS1 (PDB_1BCP, cyan). NAD^+-binding pose from Q116/E118 mutant structure of pertussis-like toxin from *E. coli* (PDB_4Z9D) was superimposed on top of the wild-type structure (PDB_4Z9C, orange).

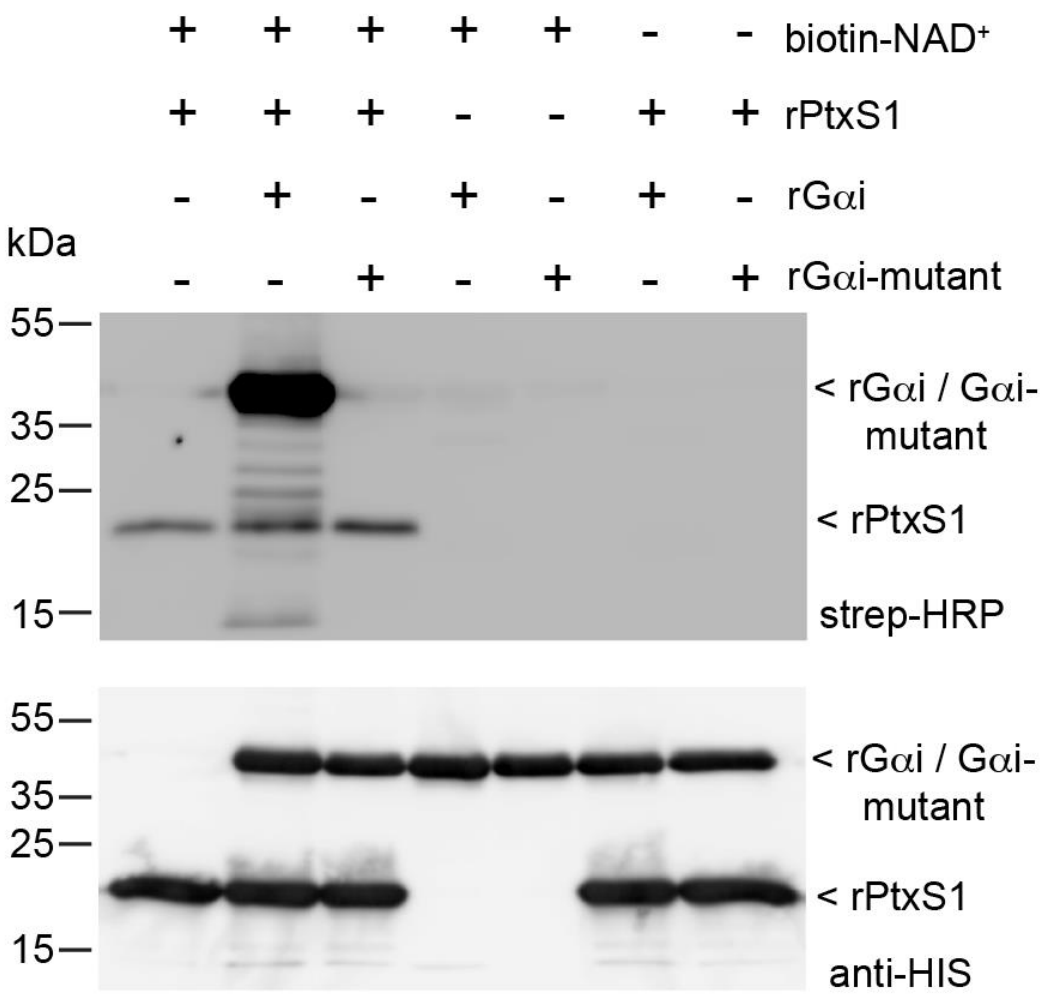

Figure S3. rPtxS1 is incapable of ADP-ribosylating a C351A-mutant of rGαi. Effect of C351A mutation to rPtxS1-catalyzed ADP-ribosylation of rGαi *in vitro* (enzyme-excess conditions). Blots probed, stripped and re-probed in the order of 1) strep-HRP and 2) anti-HIS.

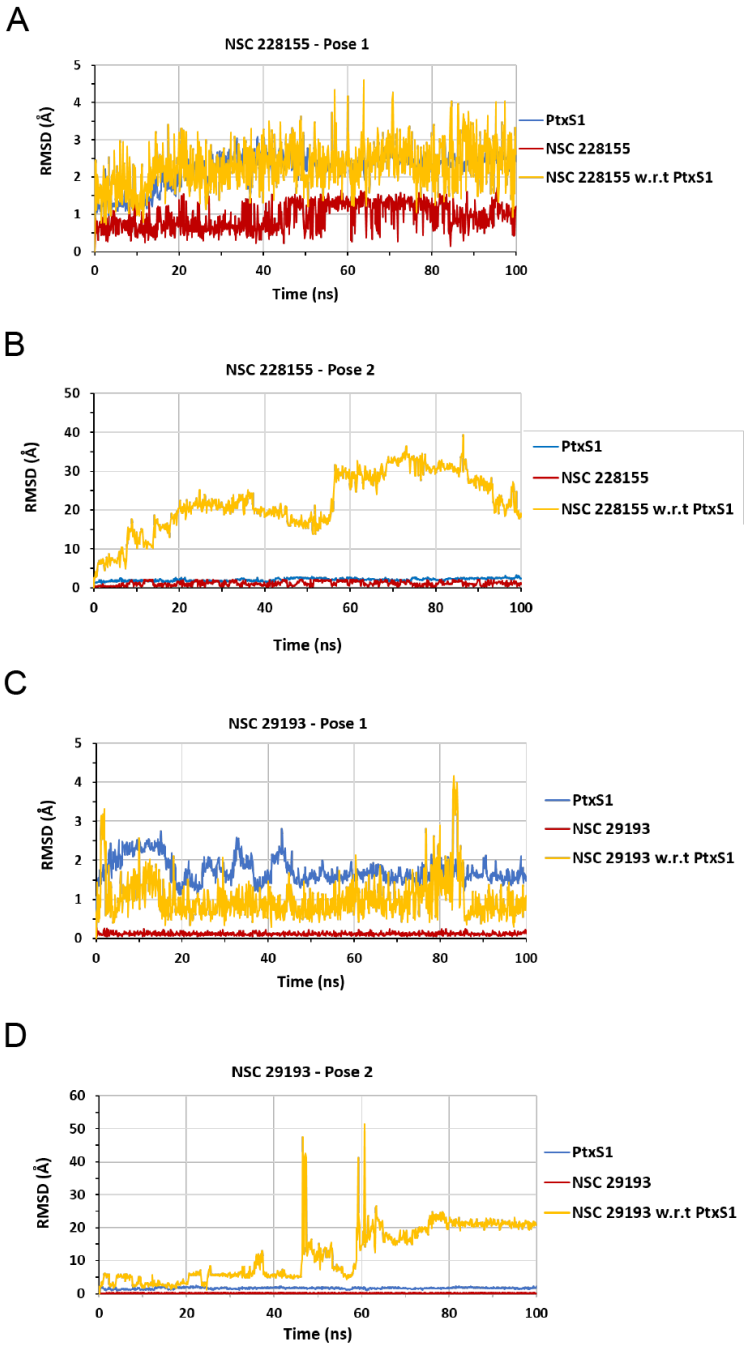

Figure S4. Molecular dynamics simulation data. Root mean square deviation (RMSD) of pose 1 **A)** and pose 2 **B)** of NSC228155 and pose 1 **C)** and pose 2 **D)** NSC29193 (see Fig. 5). Backbone atom RMSD of PtxS1 (blue) and the ligands (NSC228155 / NSC29193 - red) based on their first frame structures. Ligand RMSD (yellow) when superimposition is based on pertussis backbone atoms.

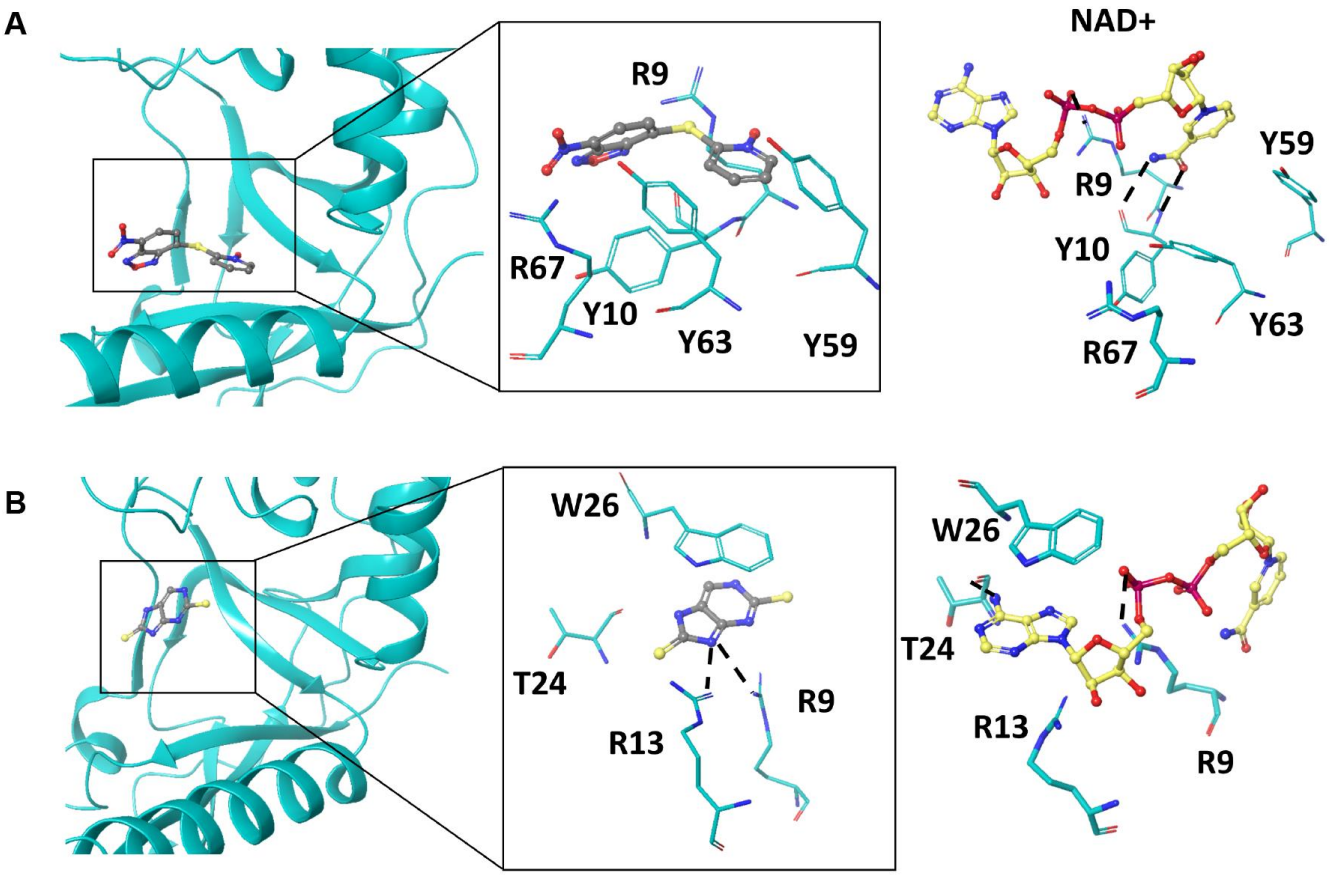

Figure S5. Prediction of binding poses of NSC228155 and NSC29193 to PtxS1. Binding pose 2 of NSC228155 (A) and binding pose 2 of NSC29193 (B) to PtxS1 (PDB_1BCP, chain A). Residues involved in ligand interactions (sticks) and hydrogen bonds (dotted lines) are shown. Binding mode of NAD^+ to PtxS1 in the corresponding area of the NAD^+-binding pocket is shown in each panel on the right (see also Fig. 1). Color-coding of atoms in NAD^+: yellow, carbon; blue, nitrogen; red, oxygen; magenta, phosphorus.

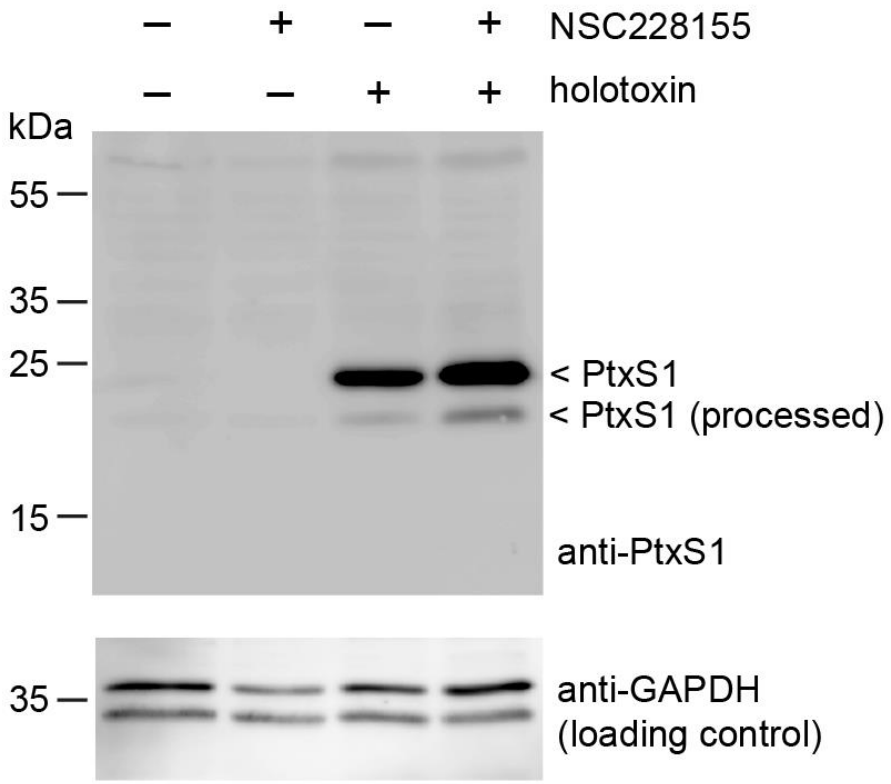

Figure S6. Effect of NSC228155 on the amount of cell associated PtxS1 and the proteolytic processing of PtxS1. NSC228155 was added 30 min before starting a 2 h incubation with the pertussis holotoxin (100 ng/mL). Same samples were probed in parallel membranes for PtxS1 and GAPDH.

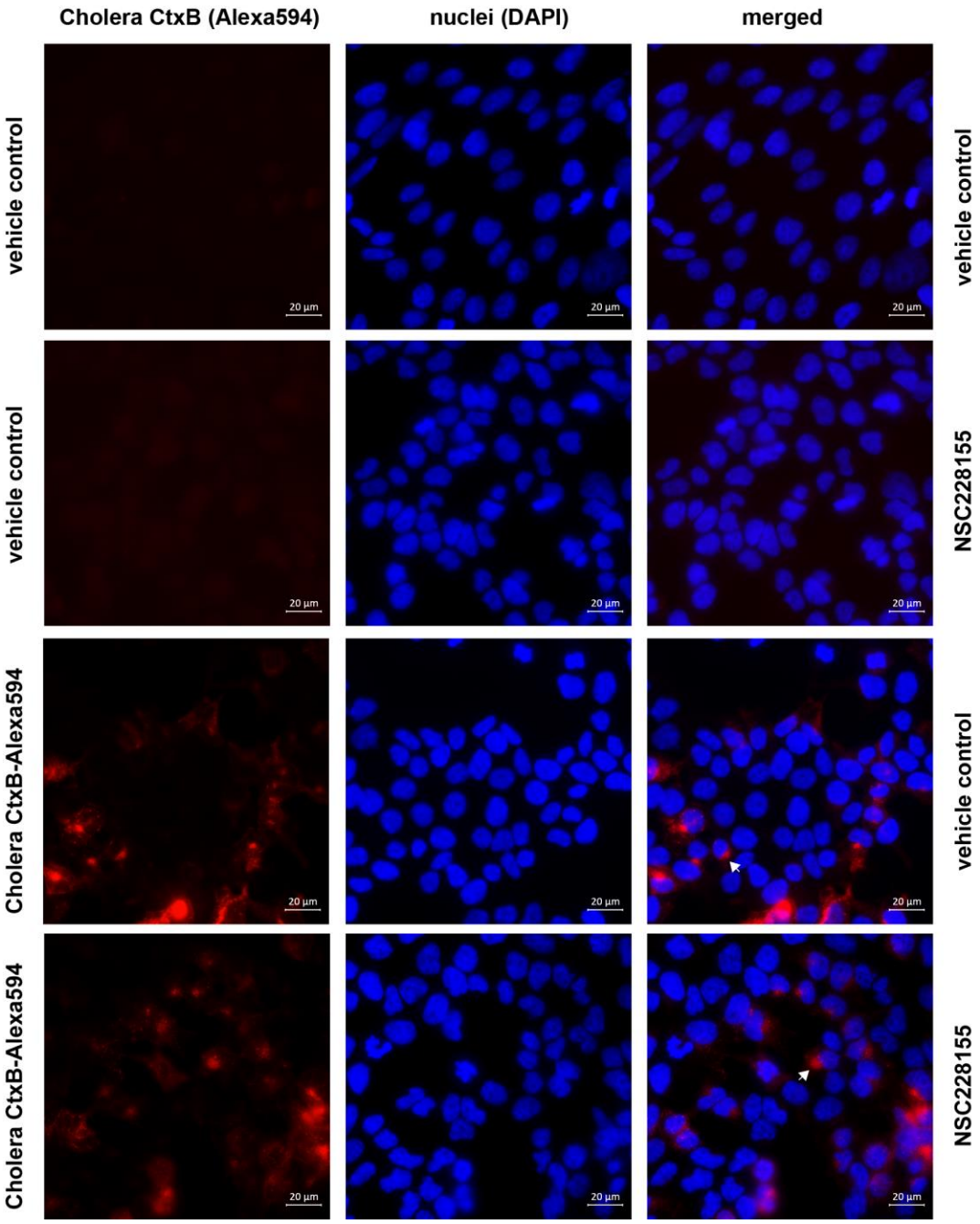

Figure S7. Effect of NSC228155 on the retrograde endosomal trafficking. 5 µM NSC228155 was added 30 min before starting a 2 h incubation with the retrograde endosomal trafficking marker cholera toxin B subunit conjugated to Alexa594 (1 µg/mL). The cells were stained for nuclei with the DNA-binding dye DAPI and imaged with an epifluorescence microscope (40x). Arrows mark examples of the typical accumulations of cholera toxin B subunit close to the nuclei.

Table S1. Assay performance statistic of the *in vitro* NAD^+ consumption assay. In order to establish repeatability of values for maximum and minimum signals between plates, wells and days, five control plates were tested. Experimental conditions and protein batches used for assay validation were the same. Three plates were made on one day while second and third days had one plate each.

Parameter	**Values**
S/B	2.60 ± 0.2
S/N	13.17±1.5
Z’	0.68±0.0
Well-to-well CV% max	3.5±0.9
Well-to-well CV% min	7.8±0.9
Plate-to-plate CV% *	1.2
Day-to-day CV% *	5.6 (5.4 – 5.9)[#]

*calculated from Z’ values

[#]indicates range for Day-to-Day CV

Table S2. ARTD/PARP inhibitory compounds analyzed for rPtxS1 inhibition.

Compound name (IUPAC)	Acronym	Supplier
3-aminobenzamide	3-AB	ALEXIS Biochemicals
Nicotinamide		ALEXIS Biochemicals
Benzamide		ALEXIS Biochemicals
2-[(2R)-2-methylpyrrolidin-2-yl]-1H-1,3-benzodiazole-4-carboxamide	Veliparib	Medchemtronica
5-amino-1,2-dihydroisoquinolin-1-one	5-AIQ	ALEXIS Biochemicals
5-amino-3-methyl-1,2-dihydroisoquinolin-1-one	3-Methyl-5-AIQ	ALEXIS Biochemicals
8-amino-3-azatricyclo[7.3.1.0^{5,13}]trideca-1(12),5,7,9(13),10-pentaene-2,4-dione	4-ANI	ALEXIS Biochemicals
5-[4-(piperidin-1-yl)butoxy]-1,2,3,4-tetrahydroisoquinolin-1-one	DPQ	ALEXIS Biochemicals
2-methyl-1H,4H,5H,7H,8H-thiopyrano[4,3-d]pyrimidin-4-one	DR2313, DRL	ALEXIS Biochemicals
2-(4-{[(2S,3S,4R,5R)-5-(6-amino-9H-purin-9-yl)-3,4-dihydroxyoxolan-2-yl]carbonyl}piperazin-1-yl)-N-(1-oxo-2,3-dihydro-1H-isoindol-4-yl)acetamide	EB-47	ALEXIS Biochemicals
1,4-dihydroquinazolin-4-one	4-Hydroxyquinazoline	ALEXIS Biochemicals
6-amino-5-iodo-2H-chromen-2-one	INH2BP	ALEXIS Biochemicals
5-hydroxy-1,2-dihydroisoquinolin-1-one	1,5-Isoquinolinediol	ALEXIS Biochemicals
(2E,4S,4aS,5aR,12aS)-2-[amino(hydroxy)methylidene]-4,7-bis(dimethylamino)-10,11,12a-trihydroxy-1,2,3,4,4a,5,5a,6,12,12a-decahydrotetracene-1,3,12-trione	Minocin	ALEXIS Biochemicals
8-hydroxy-2-methyl-1,4-dihydroquinazolin-4-one	NU1025, 4PAX	ALEXIS Biochemicals
5,6-dihydrophenanthridin-6-one	phenanthridone	ALEXIS Biochemicals
2-(dimethylamino)-N-(6-oxo-5,6-dihydrophenanthridin-2-yl)acetamide	PJ-34, P34	ALEXIS Biochemicals
4H,5H-thieno[2,3-c]isoquinolin-5-one	TIQ-A	ALEXIS Biochemicals
1,7-dimethyl-2,3,6,7-tetrahydro-1H-purine-2,6-dione	1,7-dimethylxanthine	Sigma
3-(4-chlorophenyl)quinoxaline-5-carboxamide	CNQ	Calbiochem / WVR
4-({3-[(4-cyclopropanecarbonylpiperazin-1-yl)carbonyl]-4-fluorophenyl}methyl)-1,2-dihydrophthalazin-1-one	Olaparib	Medchemtronica
(4Z)-4-[(1-methyl-1H-pyrrol-2-yl)methylidene]-1,2,3,4-tetrahydroisoquinoline-1,3-dione	BYK204165	Sigma
2-[4-(trifluoromethyl)phenyl]-1H,4H,5H,7H,8H-thiopyrano[4,3-d]pyrimidin-4-one	XAV939	Maybridge
2-(pyridin-2-yl)-5H,7H,8H-thiopyrano[4,3-d]pyrimidin-4-ol	RF03877	Maybridge
2-cyclopropyl-5H,7H,8H-thiopyrano[4,3-d]pyrimidin-4-ol	RF03876	Maybridge
4-[(1R,2S,6R,7S)-3,5-dioxo-4-azatricyclo[5.2.1.0^{2,6}]dec-8-en-4-yl]-N-(quinolin-8-yl)benzamide	IWR-1	Sigma
N-(6-methyl-1,3-benzothiazol-2-yl)-2-({4-oxo-3-phenyl-3H,4H,6H,7H-thieno[3,2-d]pyrimidin-2-yl}sulfanyl)acetamide	IWP-2	Sigma
4-iodo-3-nitrobenzamide	Iniparib	Selleck Biochemicals
6-fluoro-2-{4-[(methylamino)methyl]phenyl}-3,10-diazatricyclo[6.4.1.0^{4,13}]trideca-1,4(13),5,7-tetraen-9-one	Rucaparib, AG014699	Medchemtronica
1-oxo-1,2-dihydroisoquinolin-5-yl benzoate	UPF1035	Enzo Life Sciences
5-(2-oxo-2-phenylethoxy)-1,2-dihydroisoquinolin-1-one	UPF1069	Enzo Life Sciences
2-phenyl-4H-chromen-4-one	Flavone	Sigma